MHD Stability of Helical Modes in a Cylindrical Tokomak Plasma

W.Grossmann, S.Ortolani

IPP 1/132 April 1973

MAX-PLANCK-INSTITUT FÜR PLASMAPHYSIK

GARCHING BEI MÜNCHEN

MAX-PLANCK-INSTITUT FÜR PLASMAPHYSIK

GARCHING BEI MÜNCHEN

MHD Stability of Helical Modes in a Cylindrical Tokomak Plasma

W.Grossmann, S.Ortolani

IPP 1/132 April 1973

Die nachstehende Arbeit wurde im Rahmen des Vertrages zwischen dem Max-Planck-Institut für Plasmaphysik und der Europäischen Atomgemeinschaft über die Zusammenarbeit auf dem Gebiete der Plasmaphysik durchgeführt.

IPP 1/132

W. Grossmann
S. Ortolani*

MHD Stability of Helical Modes in a Cylindrical Tokomak Plasma

(in English)

April 1973

Abstract:

The consideration of realistic current density profiles and more exact treatment of MHD stability leads to results which can be considerably different from those previously obtained. By numerically integrating the linearized ideal MHD equations of motion more detailed and informative results can be obtained than by using the energy integral together with restrictive expansions and arbitrary test functions. We find for a cylindrical Tokomak-like plasma with a peaked on axis current distribution that $q = 1$ at the limiter is not the stability condition but that q must be much greater than unity for stability to $m = 1$ perturbations. Further it is shown that a conducting shell has a negligible effect on $m \geq 2$ modes for an on-axis peaked current distribution.

*Centro di Studio sui Gas Ionizzati - C.N.R.-
Università di Padova, Italy.

I. Introduction

The purpose of the present report is to investigate linearized MHD stability for a class of diffuse plasma profiles which are currently thought to exist in Tokomak experiments.

We place particular emphasis on the variation of the axial current density profile and the form of this profile is adjusted in such a manner to correspond to various instants of time during a typical Tokomak discharge. For example, we choose three different types of profiles:

1) the current density is peaked off the plasma axis corresponding to an early phase with "skin effect",

2) the current density is a smooth function, more or less constant over the central part of the plasma and goes to zero smoothly at the limiter;

3) the current density is peaked on the axis representing later phases noticed during recent ST discharges /6/. We find that the form of the current density profile plays a very important role in the stability of helical modes, in contradiction to earlier estimates of Shafranov /7/. The differences result from the methods by which stability is investigated. We show that the method used by Shafranov leads to optimistic results concerning Tokomak stability: more exact treatment of the problem lessens the optimism and brings the theoretical predictions more in line with the experimental findings.

One of the most well known stability criteria for plasma stability considerations is the Kruskal-Shafranov condition /8,9/. This condition states that if the rotational transform of the magnetic field on the plasma surface is greater than or equal to unity then the plasma column will be unstable to a helical shift in the radial direction. In cylindrically symmetric geometry, violation of the Kruskal Shafranov condition triggers the $m = 1$ instability (m refers to the fourier decomposition of plasma perturbations according to $\exp(i m \theta)$. The $m = 1$ instability

has long been considered to be the most dangerous mode for highly compressed, high-β pinched plasmas, /10,11/. The Kruskal-Shafranov condition, originally found in straight geometry, has been shown also to be valid in toroidal geometry, /12/.

Among the many differences between our model and the real plasma is the fact that we treat a straight cylindrical plasma instead of the fully toroidal case. We know, however, from experience that the stability of helical or kink modes in many toroidal pinch experiments follows closely the stability behaviour as predicted by an analysis performed on a straight system, /1-5/. We treat a strictly straight system and assume that the axial magnetic field is constant over the plasma and surrounding region. This is not necessarily a restriction for we show how to include poloidal currents in the calculations.

As mentioned above, the $m = 1$ instability has often been observed in pinch plasma experiments and it was, until recently, a puzzle why the higher $m \geq 2$ modes were not observed. Freidberg, /13/, has shown that finite Larmor radius effects are sufficient to suppress the growth rates for the $m \geq 2$ modes, especially in plasmas with typical Scyllac parameters. However, in devices where the Larmor radius of the ions is very small compared with the dimensions of the plasma, as is certainly the case for present day Tokomak plasmas, the $m \geq 2$ modes should be and in fact are observed, /6, 14/.

As mentioned by Mirnow, /14/, the $m = 1$ mode appears to be the most dangerous for Tokomak plasmas in so far as it is the mode which leads to a macroscopic disruption of the plasma column.

The instabilities to which we have alluded above refer to helical or kink modes of a plasma column. This definition applys to plasma perturbations which can, in cylindrical geometry, be fourier decomposed according to:

$$\vec{\xi} = \vec{\xi}(r) \exp i\,(m\,\theta + k\,z),$$

where $\vec{\xi}$ represents the distortion of the equilibrium plasma column and θ and z refer to the azimuthal and longitudinal directions respectively; k is the wavenumber of the perturbation.

As mentioned earlier, Shafranov, /7/, has treated the above defined kink modes in cylindrical geometry for plasma profiles which are claimed to simulate Tokomak profiles. Using the well-known energy principle Shafranov investigates the MHD stability of the Tokomak profiles by choosing certain functional forms for the plasma perturbation $\vec{\xi}$. Since the energy integral can be written in such a form that it only depends upon the equilibrium field quantities and the radial part of the perturbation ξ_r, a simple choice of ξ_r as a function of radius allows analytic results for such information as the marginal stability criteria and growth rates for unstable modes. Such an arbitrary specification of ξ_r can lead to completely different results than those obtained from solving the corresponding Euler-Lagrange equations for ξ_r obtained by formally minimizing the energy integral. The essential general results of Sharanov's calculation are as follows:

1) the form of the current density profile does not play a role for the m = 1 instability.
2) Sufficient for stability to m = 1 is that q > 1 (q is defined as 2 π divided by the rotational transform) at the edge of the plasma.

3) modes with $m > 2$ can be stabilized by bringing a conducting wall to the edge of the plasma;

4) a current density profile which is peaked on the axis can be found which stabilizes $m \geq 2$ modes.

We mention briefly here that there has been no experimental evidence in Tokomak experiments to support the theoretical predictions of Shafranov; on the contrary there has been evidence given /6,14/, which in fact contradicts the above predictions. We will show that the arbitrary choice of plasma perturbation leads to incorrect results and that a self-consistent treatment of the proper eigen-boundary-value problem alters the 4 above given statements. As mentioned earlier, our results fall more in line with the experimental observations.

We give next the mathematical details of the MHD stability calculations.

II. Mathematical Details

We treat the ideal MHD equations without displacement currents as our governing system. These equations are given below for completeness. They are:

Equation of continuity

$$\frac{\partial \rho}{\partial t} + \nabla \cdot \rho v = 0, \tag{1}$$

equation of momentum

$$\rho \frac{Dv}{Dt} = - \nabla P + J \times B , \tag{2}$$

equation of state

$$P = P(\rho), \tag{3}$$

Maxwell's equations,

$$\nabla \times \underset{\rightarrow}{E} = - \frac{\partial B}{\partial t} , \tag{4}$$

$$\nabla \times \underset{\rightarrow}{B} = \mu_o \underset{\rightarrow}{J} , \tag{5}$$

$$\nabla \cdot \underset{\rightarrow}{B} = 0 \tag{6}$$

and Ohm's law

$$\underset{\rightarrow}{E} = - \underset{\rightarrow}{v} \times \underset{\rightarrow}{B}. \tag{7}$$

In the above equations ρ is the plasma density, $\underset{\rightarrow}{v}$ the velocity, P the pressure, $\underset{\rightarrow}{J}$ is the current density, $\underset{\rightarrow}{B}$ is the magnetic field strength, $\underset{\rightarrow}{E}$ the electric field strength, and μ_o is the free space permeativity. The total derivative with respect to time is defined as:

$$\frac{D}{Dt} = \frac{\partial}{\partial t} + \underset{\rightarrow}{v} \cdot \nabla \tag{8}$$

In the following, the equilibrium plasma quantities will be given the subscript $(\ )_o$ and all perturbation quantities the subscript $(\ )_1$. We choose a cylindrically symmetric plasma equilibrium defined by:

$$\nabla \left(P_o + \frac{B_o^2}{2\mu_o}\right) = \frac{B_o}{\mu_o} \cdot \nabla B_o \tag{9}$$

where $B_o = (0, B_{\theta,o}, B_{z,o})$. Eqation 9 represents a static equilibrium. In appendix A is given the modification of the governing equations when a uniform rotation is allowed in the equilibrium state. We next choose the adiabatic equation of state for equation 3. It is well known that for plasma configurations where $B_{\theta,o}^2 \ll B_{z,o}^2$ the effect of compressibility plays hardly a noticeable role in the stability /15,16/. For completeness however - we give the full compressible equations here and later specialize to our particular case. We now use the assumption that small perturbations of the plasma equilibrium have the form:

$$\phi_1 = \phi_1(r) \exp\left[\gamma t + i(m\theta + k z)\right] \tag{10}$$

where ϕ represents any perturbation quantity. Equations (1 - 7) are now expanded and under the assumption that perturbation velocity components can be written as:

$$\underset{\rightarrow}{v}_1 = \frac{\partial \underset{\rightarrow}{\xi}_1}{\partial t} \tag{11}$$

where $\underset{\rightarrow}{v}_1$ is the perturbed velocity and $\underset{\rightarrow}{\xi}_1$ is Lagrangian coordinate representing the shift of the plasma away from the equilibrium we obtain the following equations for $\xi_{r,1}$ $\xi_{\theta,1}$, $\xi_{z,1}$ and P_1^* as:

$$\left[\rho_o\gamma^2 + \frac{F^2}{\mu_o} - \frac{2B_{\theta,o}}{\mu_o}\left(\frac{B_{\theta,o}}{r}\right)'\right]\xi_{r,1} + \frac{2 i F B_{\theta,o}}{\mu_o r}\xi_{\theta,1} + P_1^{*\prime} +$$

$$- \frac{2 B_{\theta,o}^2}{\mu_o r} \nabla \cdot \underset{\rightarrow}{\xi}_1 = 0, \tag{12}$$

$$\left[\rho_o \gamma^2 + \frac{F^2}{\mu_o}\right]\xi_{\theta,1} - \frac{2 i F B_{\theta,o}}{\mu_o r}\xi_{r,1} + \frac{im}{r} P_1^* + \frac{i F B_{\theta,o}}{\mu_o} x$$

$$\nabla \cdot \xi_1 = 0. \tag{13}$$

$$\left[\rho_o \gamma^2 + \frac{F^2}{\mu_o}\right]\xi_{z,1} + i k P_1^* + \frac{i F B_{z,o}}{\mu_o} \nabla \cdot \underset{\rightarrow}{\xi}_1 = 0, \tag{14}$$

$$P_1^* = \frac{iF}{\mu_o} \underset{\rightarrow}{B}_o \cdot \underset{\rightarrow}{\xi}_1 + \frac{2 B_{\theta,o}^2}{\mu_o r}\xi_{r,1} - \left(\Gamma P_o + \frac{B_o^2}{\mu_o}\right) \nabla \cdot \underset{\rightarrow}{\xi}_1, \tag{15}$$

where in the above Γ is the specific heat ratio, $F = \frac{m}{r} B_{\theta,o} + k B_{z,o}$, and the prime denotes differentiation with respect to r. P_1^* is the total perturbed plasma pressure. Equations (12 - 15) can be combined to yield two first order differential equations for $\xi_{r,1}$ and P_1^* as:

$$\left(r\,\xi_{r,1}\right)' = \left[\frac{2\,m\,F\,B_{\theta,o}}{\mu_o\,r^2\,A} - \frac{2\,B_{\theta,o}^{\,2}}{\mu_o\,r}\,\Lambda\right]\left(r\,\xi_{r,1}\right)$$

$$-\frac{1}{r^2}\left[r\,\frac{(m^2+k^2r^2)}{A} - r^3\,\Lambda\right]\,P_1^{\,*}, \qquad (16)$$

$$\left(P_1^{\,*}\right)' = \frac{1}{r}\left[-A + \frac{2\,B_{\theta,o}}{\mu_o}\left(\frac{B_{\theta,o}}{r}\right)' + \frac{4\,B_{\theta,o}^{\,2}F^2}{\mu_o^{\,2}\,r^2\,A}\right.$$

$$\left. - \frac{4\,B_{\theta,o}^{\,4}}{\mu_o^{\,2}\,r^2}\,\Lambda\right]\left(r\,\xi_{r,1}\right) -$$

$$\left[\frac{2\,m\,F\,B_{\theta,o}}{\mu_o\,r^2\,A} - \frac{2\,B_{\theta,o}^{\,2}}{\mu_o\,r}\,\Lambda\right]P_1^{\,*}. \qquad (17)$$

In the above the following definitions apply for A and Λ :

$$A = \rho_o\,\gamma^2 + \frac{F^2}{\mu_o}, \qquad (18)$$

$$\Lambda = \begin{cases} 0\ , \text{ for incompressible modes } \nabla\cdot\underset{\sim}{\xi}_1 = 0 \\ \dfrac{-\gamma^4\rho_o^{\,2}}{A^2\left[\Gamma P_o + \dfrac{B_o^{\,2}\gamma^2\rho_o}{\mu_o A}\right]}\ , \text{ for compressible modes } \nabla\cdot\underset{\sim}{\xi}_1 \neq 0 \end{cases}$$

In the following we treat only incompressible modes, $\Lambda = 0$, and remark that compressibility effects have been shown to affect our results by less than several percent in the calculated growth rates. The marginal stability boundaries, as is well known, are not changed by compressibility effects. With $\Lambda = 0$, the above two equations, (16 - 17), can be combined into one second order differential equation for $\xi_{r,1}$. This is the equation originally

used by Freidberg to study the stability of a diffuse screw pinch /17/. We now drop the subscripts $(\,)_1$ for $\xi_{r,1}$ and $(\,)_o$ for the quantities ρ_o, $B_{\theta,o}$ and $B_{z,o}$ and give the second order differential equation for ξ_r as:

$$\left[a \, (r \, \xi_r)' \right]' - b \, \xi_r = 0, \tag{20}$$

where: $$a = \frac{r \, A}{m^2 + k^2 r^2}, \tag{21}$$

and, $$b = A - \frac{2 B_\theta}{\mu_o} \left(\frac{B_\theta}{r} \right)' + \frac{2 m r}{\mu_o} \left(\frac{F \, B_\theta}{r(m^2+k^2r^2)} \right)'$$

$$- \frac{4 k^2 F^2 B_\theta^2}{\mu_o^2 \, A(m^2+k^2r^2)} \, . \tag{22}$$

An expansion of 20) about the origin yields the boundary condition for ξ_r at the origin. It is found for $m \geq 1$ that

$$\xi_r \sim r^{m-1} \tag{23}$$

for small r. With equation 23) we have enough information to integrate equations 16) and 17) away from the origin. The problem we solve is as follows.

Given an equilibrium profile, ρ, B_θ and B_z as functions of r, we integrate 16) and 17) numerically, for an initial choice of γ, the eigenvalue, up to a specified value of r representing either the plasma surface or a perfectly conducting wall. Iteration on γ is performed until a prescribed boundary condition on ξ_r is fulfilled. For a perfectly conducting wall the boundary condition requires that ξ_r vanish at the wall.

The differential equations (16 - 17) are conveniently non-dimensionalized by the following variables. Let us define a radius R_L which shall denote the outermost radius or extent of the axial current density profile. Later we shall use the term

limiter to define R_L. We define a parameter μ (see Freidberg /17/) as:

$$\mu = \frac{B_\theta(R_L)}{B_o} = \frac{\mu_o I_z}{2\pi R_L B_o} , \tag{24}$$

and we take B_o to be the constant axial magnetic field. Defining further :

$$\tilde{r} = \frac{r}{R_L} , \; B_z = f_1(\tilde{r})\, B_o ,$$
$$B_\theta = \mu B_o f_2(\tilde{r}) , \; \tilde{\gamma} = \frac{\gamma R_L \sqrt{\rho \mu_o}}{\mu B_o} \tag{25}$$

where $f_1(\tilde{r})$ and $f_2(\tilde{r})$ are then form factors for the radial dependence of the z and θ magnetic fields. If we now consider a topological torus, that is, we give a periodicity condition for the cylinder then we can define R_T, the torus radius, such that $2\pi R_T$ is the length of the cylinder we are considering. With this definition we can define the parameter q (see Shafranov /7/) as:

$$q = \frac{r B_z}{R_T B_\theta} = \frac{R_L}{R_T} \frac{1}{\mu} \frac{\tilde{r} f_1(\tilde{r})}{f_2(\tilde{r})} = q(R_L) \frac{\tilde{r} f_1(\tilde{r})}{f_2(\tilde{r})} \tag{26}$$

For the wavelength k we can define the following dimensionless variable $\tilde{k}$ as:

$$\tilde{k} = \frac{k R_L}{\mu} = \frac{N R_L}{\mu R_T} = N q(R_L) . \tag{27}$$

The variables $\tilde{k}$ and N for a given value of $q(R_L)$ will be interchangeably used.

The above parameters will allow us to draw important comparisons between the results for the various profiles. We describe next the Tokomak models used for the present calculations.

III. The Tokomak Models

As mentioned earlier, we will consider the effect of various axial current density profiles. We choose the axial magnetic field to be identically a constant so that B_o and f_1 in equation 25) become the constant magnetic field strength and unity respectively. We choose a density profile which has been the most often reported from experiments:

$$\rho = \rho(o) \quad (1 - \tilde{r}^{\,4}), \tag{28}$$

where $\rho(o)$ is the density on the axis. Next we give the current density profiles which we consider.

Profile I This profile corresponds to the case where a sheath exists and models the so-called "skin effect". The current density is given as:

$$J_z^I(\tilde{r}) = a_I \exp\left[- \alpha \mid \tilde{r} - \tilde{r}_o \mid\right], \quad \alpha = \text{constant}, \tag{29}$$

where a_I is a constant related to the total current and where $\tilde{r}_o$ is some radial position between the center of the plasma and R_L. For this profile we have:

$$\tilde{r} \le \tilde{r}_o \,, \quad f_2^I(\tilde{r}) = \frac{1}{\tilde{r}} \; \frac{(\alpha\,\tilde{r} - 1)\, e^{\alpha(\tilde{r}-\tilde{r}_o)} + e^{-\alpha\tilde{r}_o}}{T_I}, \tag{30}$$

$$\tilde{r} > \tilde{r}_o, \quad f_2^I(\tilde{r}) = \frac{1}{\tilde{r}} \; \frac{2\,\alpha\tilde{r}_o + e^{-\alpha\tilde{r}_o} - (1+\alpha\tilde{r})\, e^{-\alpha(\tilde{r}-\tilde{r}_o)}}{T_I}, \tag{31}$$

where

$$T_I = 2\,\alpha\tilde{r}_o + e^{-\alpha\tilde{r}_o} - (1+\alpha)\, e^{-\alpha(1-\tilde{r}_o)}, \tag{32}$$

Necessary for the numerical method is the derivative of $f_2(\tilde{r})$ near the origin. This turns out to be:

$$f_2^{I\,\prime}(o) = \frac{\alpha^2\, e^{-\alpha\tilde{r}_o}}{2\,T_I}. \tag{33}$$

in the following r_o will chosen to be 0.8.

Profile II This profile is more or less uniform over the central portion of the plasma and vanishes uniformly at $r = R_L$.

We choose:

$$J_z^{II}(\tilde{r}) = a_{II}\ (1 - \tilde{r}^n) \tag{34}$$

where again a_{II} is related to the total current. The function $f_2(\tilde{r})$ becomes:

$$f_2^{II}(\tilde{r}) = \frac{n+2}{n}\,\tilde{r}\ \left(1 - \frac{2}{n+2}\,\tilde{r}^n\right), \tag{35}$$

and

$$f_2^{II\prime}(o) = \frac{n+2}{n}\ . \tag{36}$$

In the following we choose n = 4.

Profile III This profile corresponds to the case where the current density is peaked on the axis. Here we choose

$$J_z^{III}(\tilde{r}) = a_{III}\ \exp\ (-\alpha\tilde{r}), \qquad \alpha = \text{constant} \tag{37}$$

and solving for $f_2(\tilde{r})$ yields

$$f_2^{III}(r) = \frac{1}{\tilde{r}}\ \frac{1 - (1+\alpha\tilde{r})e^{-\alpha\tilde{r}}}{T_{III}}\ , \tag{38}$$

and

$$f_2^{III\prime}(o) = \frac{\alpha^2}{2T_{III}}, \tag{39}$$

where:

$$T_{III} = 1 - (1+\alpha)e^{-\alpha}\ . \tag{40}$$

Profile IV This profile is essentially the same as profile III; the value of α will be chosen larger than that of III to emphasize the effect of the current density peaking on the axis.

We mention here that the calculations with all profiles are made with a constant value of total current. Shown in figure 1 are the typical current density profiles normalized to their maximum values. For the profiles I and IV the value of α is chosen to be 5 whereas for III the value of α is 3. All current density profiles terminate at $\tilde{r} = 1$ which we define as the limiter position. Outside the limiter, vacuum magnetic fields are assumed to exist. Shown in figure 2 are the typical profiles for $f_2(\tilde{r})$ for the four different current density profiles. At the limiter position, $\tilde{r} = 1$, notice that the poloidal magnetic field strength for all cases is the same. Shown also is the tendency towards more vacuum field like profiles the more localized the current density is on the axis. According to the results of Freidberg, /17/, one would expect that the more vacuum like profiles should be the most unstable; this is essentially what we will show here in this report.

We wish to specialize our model Tokomak even further as follows. We choose the following parameter values for our plasma:

$$R_L = 10 \text{ cm}, \quad R_T = 50 \text{ cm}$$

$$B_o = 20 \text{ k Gauss}, \quad I_z = 200 \text{ k amperes}$$

such that $\mu = 0.2$

and $q(R_L) = 1$

We choose further:

$$n(o) = 10^{13} \text{ cm}^{-3}$$

where $n(o)$ is the centerline plasma particle density. This choice of $n(o)$ leads to:

$$\tilde{\gamma} = .5 \times 10^{-7} \gamma. \tag{42}$$

finally we have that:

$$\tilde{k} = 50\ k\ = N \qquad (43)$$

It should be noticed that many of the above given parameters can be varied, holding μ and $q(R_L)$ constant, over a wide range representative of present day Tokomak experiments.

It is now instructive to show the radial profile of $\tilde{q}(\tilde{r})$ for the different cases. Shown in figure 3 is just this information. It is seen that for the plasma profile with current peaked off axis that $\tilde{q}$ is a monotone decreasing function of radius. In this case the rotational transform increases with radius. In all other cases (profiles II, III and IV) the q profile is a monotone increasing function of $\tilde{r}$. In these cases the rotational transform decreases monotonely with $\tilde{r}$. As shown, the value of $\tilde{q}$ at the limiter ($\tilde{r} = 1$) is fixed at unity. All curves in figure 3 can be uniformly shifted in the vertical direction by changing either the total current, the axial magnetic field strength or the aspect ratio (R_T / R_L).

Another instructive property of the various plasma profiles are so-called singular or resonant surfaces. These surfaces are defined by the position where the plasma perturbation (ξ) is exactly perpendicular to the magnetic surface. These singular surfaces can be found by setting F, defined in equations (12 - 15) and equal to $\underset{\rightarrow}{k} \cdot \underset{\rightarrow}{B}_o$, identically equal to zero. For the scaling parameters used in our calculations, equations(26 and 27), setting F equal to zero results in

$$q(R_L)\ \frac{N}{m} = -\ \frac{1}{\tilde{q}(\tilde{r})}, \qquad (44)$$

where m is again the poloidal mode number of the perturbation and N is periodicity number of the perturbation wavelength. (N = 1 represents one full wavelength in the topological torus). In equation 44) $q(R_L)$ should be set equal to unity

for the choice of $\mu = .2$ and $R_T/R_L = 5$. We see in figure 4 that for profile I only a relatively small region in $(N/m)q(R_L)$ contains resonant surfaces. The same is observed for profile II. For the profiles III IV it is shown that larger regions containing resonant surfaces open up. For all cases it is noticed that for our Tokomak model ($q(R_L) = 1$) and for m=1 that N=1 is resonant at the limiter. We leave the significance of these curves to a later discussion and give now another property of the different profiles. First we write the Suydam condition, which if violated is a sufficient condition for instability, in terms of the current density as:

$$-\frac{8\mu_o}{B_o^2}\frac{J_z}{\tilde{r}^2}\left[\int_o^{\tilde{r}} J_z(\tilde{r}')\,\tilde{r}'\,d\tilde{r}'\right] + \tilde{r}^2\left[J_z - \frac{2}{\tilde{r}^2}\int_o^{\tilde{r}} J_z(\tilde{r}')\tilde{r}'d\tilde{r}'\right] \geq 0. \tag{45}$$

where the B_z-field has been held constant and equal to B_o.

From equation 45) it is seen that the region of the plasma cross section where the Suydam condition is not fulfilled follows the position where the current density is peaked or localized. For example, shown in figure 4 is a region labled 1 which represents the portion of the plasma radius for profile I where the Suydam condition is violated. The region 1 is located near the edge of the plasma outside of the position where the current density profile is peaked. Region 2 is the corresponding Suydam unstable region for profile II. For profile II, the current density has its maximum on the axis and hence the region where equation 45) is not satisfied begins at the axis. The same behaviour is noticed for profiles III and IV with the feature that as the current density becomes more peaked the Suydam unstable region shrinks to a narrow region around the origin. It will shown later that when the marginal stability boundaries fall within a region where the violation of equation 45) is localized, localized perturbations are found.

We turn next to a discussion of the results of the stability calculations using the above described plasma profiles.

IV. Results

In this section we present the results from the numerical computations of growth rates for the instabilities for the plasma profiles which were described in the previous section.

As a check on the accuracy of our numerical calculations, a set of analytical results obtained by R.J.Tayler,/18/, for constant pitch plasma profiles given as:

$$\begin{aligned} B_z &= C_1, \\ B_\theta &= C_2\, r, \\ \rho &= C_3 \end{aligned} \tag{46}$$

(where C_1, C_2, and C_3 are constants) were compared with numerical computations using the above profiles and the method described here. Shown in figure 5 is the envelope of the $\tilde{\gamma}$ versus $\tilde{k}$ for incompressible m=1 modes. The comparison between the analytical results of Tayler which are an exact solution for the dispersion relation and the numerical computations obtained by integrating the governing differential equations is correct to three decimal places. This agreement allows confidence in the present technique. We mention here that the Tayler profiles have been extensively examined by a number of authors, /15,16/, and it has been shown that for these constant pitch profiles the effect of compressibility considerably alters the $\tilde{\gamma}$ versus $\tilde{k}$ spectrum. A discussion of these interesting but somewhat academic considerations can be found in /20/.

For the plasma parameters mentioned earlier the growth rates versus N, the wave period number, for the m=1 mode are shown in figure 6. Shown in the figure is the growth rate in μs versus N for profiles I - IV. The most striking feature of the resulting graphs is the fact that the maximum growth rate is higher the more peaked the current density profile is towards the center of the plasma. Further, the maximum growth is found for higher N the more peaked the plasma current is on the axis. In figure 6 is shown the difference obtained when two cases of plasma boundaries are treated. For the fixed boundary case, that is, assuming that the limiter is replaced with a perfectly conducting wall (the right hand portion of the curves joined with the dashed curve) one notices that as the current density peaks near the outer edge of the plasma and as it thus approaches the sharp boundary case the limit $q(R_L) = 1$, $N = 1$ is exactly obtained. On the other hand, if an external region is added to the plasma by removing the perfectly conducting wall to a position outside the limiter position (the full curves including the portion to the left of the dashed curves) it is seen that additional long wavelength modes become unstable. For profile IV the external region adds only a small correction to the growth rate curve and does not affect the maximum growth rate. However, much more important than this is the fact that the instability around N=1 becomes much more unstable with a growth rate an order of magnitude larger than the corresponding fixed boundary case.

For the remaining profiles, I - III, the addition of an external region plays a very important role in that the maximum growth rate is controlled by the position of the conducting wall. Again it is seen that by addition of an external region a range of longer wavelengths become unstable.

If we restrict our attention to N=1, the theoretically longest wavelength which can fit into the topological torus, in all cases, I - IV, the external region has a strong effect on the stability of the m=1 mode. In figure 6, for the free boundary calculations, the position of the conducting wall was taken to be 1.5 times the position of the limiter.

Before proceeding further we mention here the manner in which the external region was treated. As mentioned in /19/, there are several ways in which the external region can be treated. The possible approaches are of course dependent on the actual conditions existing outside the main portion of the plasma column. For a plasma profile which should simulate the Tokomak situation the following features should be included. First the main part of the density should vanish at the limiter position along with the termination of the current density. In the region between the limiter and the edge of the vacuum vessel a very tenuous plasma, possibly at low temperature and hence slightly conducting, along with vacuum-like magnetic field profiles should be considered. Finally the gap between the vacuum vessel and the conducting shell, resulting in true vacuum field conditions, should be considered. In the present work we do not consider the external gap and assume that the conducting wall co-incides with the vacuum vessel wall. The consequences of this choice will be discussed later. For the region between the limiter and the conducting wall we take a small but constant density and pure vacuum magnetic fields. This choice of outer region model eliminates the difficulty of handling the singular surfaces should they occur in the region between the limiter and the conducting wall. This is a very important point and will be discussed in detail later. We use the above model then for the outer region and we show in figure 7 the results of growth rate calculations and the effects on the same which come from varying the value of the small constant

density in the outside region. Shown in the figure are the values of $\tilde{\gamma}$ as a function of the ratio of external density to centerline density for the profile IV with $\mu = .2$, $\tilde{k} = .6$ and $m = 1$. Noticed in the figure is approximately a 10 percent change in the growth rate as the density ratio veries over two orders of magnitude and furthermore, convergence is observed as the external density is lowered. In the calculations mentioned above the external density ratio was held fixed at 5×10^{-4}.

The above results for the influence of the external region on m = 1 stability are not surprising. Expecially for the longer wavelengths ($\tilde{k} \leq 1$) is this behaviour to be expected since the radial eigenfunction extends over a considerable portion of the main plasma column. For instance, shown in figure 8 is a typical example of the radial eigenfunction as a function of $\tilde{r}$ for an m = 1 mode for profile IV. In the figure are shown the results for both fixed boundary (dashed lines) and free boundary (solid curves) cases. It can be seen that, for small $\tilde{k}$ the eigenfunction extends almost to the limiter with a constant value of unity (the ξ_r curves are normalized to unity at the origin for m = 1 modes) for the fixed boundary case. Relaxing the boundary condition on ξ_r at the limiter (obtained by removing the conducting wall to the position R_w) gives a finite value for ξ_r at the limiter, and, hence a larger growth rate. For the larger values of $\tilde{k}$, however, it is seen in the figure that the eigenfunction is relatively unchanged by moving the conducting wall from the position R_L to R_w. These short wavelength modes are localized near the axis and, as recalled from figure 4, appear to lie inside a region where the Suydam criterion is violated. This behaviour has been noticed before for the m = 1 instability for a class of reverse-field pinch plasma profiles /19, 21/. Indicated

in the figure is the fact that for the eigenfunctions which are localized well within the main plasma column the boundary condition on ξ_r at R_L and R_w are practically the same resulting in only fractions of a percent difference in growth rates or eigenvalue. It is this localization of eigenfunctions, shown later to be also characteristic of the $m \geq 2$ modes, that will explain the fundamental differences between our results and those of Shafranov /7/.

Let us now examine the $m = 1$ eigenfunctions for the other profiles. Shown in figure 9 are typical eigenfunctions for the various profiles for the fixed boundary case, $\mu = 0.2$. Figure 9a represents the $m = 1$ eigenfunction for profile I; the radial extent of the constant portion of the eigenfunction is almost to the wall. Although not shown in this figure, the calculated values for ξ_r for profile I actually peak at a radial position which lies within a region where the Suydam criterium is violated; region 1 in figure 4. This behaviour is consistent with results obtained by Crow and Robinson,/19/, and more recently by Ortolani,/21/. Figure 9b shows the corresponding typical eigenfunction for profile II. Here the radial extent of the constant portion is less than that of the previous profile and is for all values of $\tilde{k}$ peaked at $\tilde{r} = 0$. Figure 9c represents the typical ξ_r function for both type III and IV profiles. Here we notice that radial extent of the constant portion of the eigenfunctions is even less than that of the type III profile. Shown again in the figure 9c is the tendency of the eigenfunction to become more localized as $\tilde{k}$ or N increases. As $\tilde{k}$ becomes larger and as the region where the Suydam criterium is violated nears the marginal stability boundary, the eigenfunction becomes extremely localized. We mention here that only for the profiles III and IV is there such a strong variation of the radial eigenfunctions in the spectrum of unstable modes.

We turn our attentionnow to another aspect of the stability analysis of the various profiles. It has long been a question as to whether there exists islands of stability along the $\tilde{k}$ axis in between the regions of instability for m = 1,2 and higher modes. As shown by Shafranov, /7/, these regions exist for the constant current density case. Whereas Shafranov has chosen a constant value of $\tilde{k}$ and varies q (which in the plasma is a constant), we fix q for the calculation and vary $\tilde{k}$. It requires some effort to bring the two procedures into a close comparison, however, the reason behind the present choice will become apparent later when attempting to establish an absolute stability criterium against m = 1 for an arbitrary profile. For the present calculations it suffices to mention that the profile I case actually has regions along $\tilde{k}$ of rather wide extent where stability can be found. For the profile II case, the spectrum of unstable modes for m = 1 and 2, μ = 0.2, is shown in figure 10. Here is given the growth rate as a function of $\tilde{k}$ for the m = 1 fixed boundary case and for both the fixed and free boundary case for m = 2. It can be seen that there is a noticeable effect from the external region (circles on the curve) on the m = 2 mode tending to extend the fixed boundary growth rate curve (solid curve plus dashed portion) to lower values of $\tilde{k}$ or N. This behaviour is similar to that found for the m = 1 mode and can be understood by examining the m = 2 eigenfunctions as shown in figure 11. In the figure are shown the results for two values of $\tilde{k}$ for the fixed boundary case. As $\tilde{k}$, or N, increases the eigenfunction becomes more localized inside the plasma thus decreasing the effect of the position of an external conducting wall. For lower values of N the eigenfunction extends almost to the wall and hence leads to a noticeable destabilizing effect as the conducting wall is removed to a position outside that of the limiter. It can also be seen that the m = 2 eigenfunction varies linearly with radius $\tilde{r}$ to about 20 percent of the total radial extent. Returning to figure 10 again, it is noticed that, as in the case for profile I, stable regions in $\tilde{k}$ exist.

Figure 12 shows a different situation, however, and represents the unstable mode spectrum of profile IV for m = 1,2 and 3 modes; μ = 0.2 and fixed boundary. Here we see that the growth rate curves for m = 1 and 2 and for m = 2 and 3 overlap indicating no regions of stability in $\tilde{k}$ space to the right of the m = 1 growth rate curve. The effect of an external region on the m = 1 mode has been covered (see figure 5) and we mention here that only a very small effect can be noticed for the m = 2 mode (solid curve with the circles). Again the effect of removing the conducting wall away from the plasma is to open up longer wavelength modes to instability. The reason behind the almost negligible effect of the external region on the m = 2 mode can be found by examining the m = 2 and 3 eigenfunctions. Figure 13 shows these eigenfunctions for both small and large values of N. First it should be noticed that the eigenfunctions are very much localized well within the interior of the plasma. Furthermore, as N increases and nears the marginal stability boundary, the m = 2 and 3 eigenfunctions peak very close to the $\tilde{r}$ = 0 axis corresponding to the region where the Suydam criterium is violated. Recapitulating, the main feature of the $m \geq 2$ eigenfunctions for plasma profiles of type III and IV is a localization well within the plasma interior. The effect of an external conducting wall appears to be minimal.

In the above the value of μ has been held constant and equal to 0.2. This is equivalent to holding the total axial current constant (for constant R_L and B_o) or the ratio $I_z/R_L B_o$ constant. Figure 14 shows the results of varying the value of μ from 0.2 to 0.05 on the m = 1 mode for the fixed boundary case and for profile IV. In the figure is shown the normalized growth rate $\tilde{\gamma}$ as a function of $\tilde{k}$ or N q (R_L) for four different values of μ corresponding to four separate values of q at the limiter, q (R_L). All growth rate curves are nested in $\tilde{\gamma}$, $\tilde{k}$ coordinates. The effect of decreasing μ or say the total current, is to decrease the growth rate as expected. The maximum growth rate, however, appears to decrease linearly with decreasing μ. We

return to this point later. Shown for completeness in figure 15 are the m = 1 eigenfunctions for the four above mentioned values of μ for profile IV. The effect of decreasing μ for the smaller values of $\tilde{k}$ is to extend the region of constancy of ξ_r to larger values of $\tilde{r}$ whereas there is little effect for the larger values of $\tilde{k}$.

If, instead of presenting the data of figure 14 in terms of $\tilde{\gamma}$ and $\tilde{k}$, we plot the curves as a function of ν and k we obtain the results as shown in figure 16. In this figure we see that the effect of lowering μ is not only to lower the growth rate but to open up smaller values of k to instability. At the lower end of k it can be seen as μ is increased for a constant value of k that the m = 1 mode is at first unstable and then stable as μ exceeds a certain value.

We proceed now to a discussion of the above mentioned results.

V. Discussion of Results

In this section we will discuss the results of the numerical calculations presented above. We will attempt to compare, where possible, our results with other theoretical analyses and relevant experimental findings.

First let us recall that the present calculations were made with constant total axial current resulting in a value of q at the limiter which is the same for all four current density profiles. The reason for this choice is found in recent experiments with the Princeton ST Tokomak where the plasma current pulse is programmed to have a constant value over the main part of the discharge, /22/. Thus, after an initial phase where the plasma column is formed, our calculations should model the operation of an ST-like discharge as the current density profile (at constant total current) changes with time during the later phases of the plasma discharge.

We return now to figure 6 and to a consideration of the growth rates of m = 1 modes for the various types of axial current density profiles. In the figure it is shown that for the free boundary (plasma plus external region) situation and for the long wavelength perturbations (N ≈ 1) that a change in the current density profile affects a change in the growth rate for the m = 1 mode. For N = 1 the difference is as much as a factor of 5. For smaller N near the marginal point the difference is much less. We conclude then, depending on the wavelength of the perturbation, that the current density profile can affect the m = 1 stability. Shafranov, /7/, neglects terms of the order of $k^2 r^2$ in an energy integral analysis as being small compared with m^2, thus he is necessarily restricted to the very low end of the growth rate curve. He finds also that practically no significant effect of the current density profile can be noticed in the growth rates for m = 1 modes. If we recall the experience gained from examining high-β toroidal pinch experiments we can show that there is no reason why the plasma should choose N = 1 as the most probable unstable wavelength. As a matter of fact, as shown in /19, 20/ values of N ranging from 2 to 24 can be experimentally observed depending on the particular experiment. It could be that, in a Tokomak, the limiter plays a role in some undefind manner and restricts the possible m = 1 wavelengths to N = 1 or to low values. If this is not the case then our experience indicates that the plasma will choose the value of N corresponding to maximum growth. We mention that the maximum growth rates typical for our calculations vary from 1 μs to 100's of nanoseconds. The so-called "disruptive instability" typical of Tokomak discharges takes place on time scales of this order although it is not at all clear that this instability is an m = 1 mode, /22, 23, 24, 26/. A negative voltage spike is observed during the onset of the disruptive instability and although an m = 1 leads to the proper sign of the spike, the previously calculated growth rates of m = 1 motions /23, 24/ were too small to yields the order of magnitude of the observed voltages. The growth rates which we obtain are at least an order of magnitude higher (if one allows N > 1) and theoretically could lead

to voltage spikes of the order of several hundreds of volts. This has not been shown, however, and remains as an open question.

The next point which will be discussed is the general sufficient condition due to Shafranov, /7/, which states that the onset of an m = 1 instability is that q be less than unity at the limiter and that stability against m = 1 can be assured by fixing $q > 1$ at the limiter. Our calculations show that this is true for an exact constant current density plasma or for the singular case of a sharp boundary surface current model The following argument will show that this criterion is, in general, not valid. We recall that the profile IV growth rate variation with μ (or similarly with total current), shown in figure 14, showed a linear variation of the maximum growth with μ. This can be more dramatically demonstrated by plotting $\tilde{\gamma}_{max}$ versus μ and this is shown in figure 17. The variation is indeed linear and in the figure is also shown the variation of $\tilde{\gamma}$ as a function of μ for several values of $\tilde{k}$. Extrapolation of the linear $\tilde{\gamma}_{max}$ curve to zero growth rate yields a value of $\mu = 0.02$ for which m = 1 should be stable. Returning to figure 3 and recalculating the q profile yields for $\mu = 0.02$ the value of q = 10 at the limiter and approximately q = 0.7 on the axis. Mirnov,/14/, has suggested that a more reasonable condition for m = 1 stability (compared with Shafranov's $q(R_L) > 1$ condition) is that q should be greater than unity everywhere in the plasma. Our conclusion is that a different stability condition will be obtained depending on the current density profile. In all cases it is more than likely that q will have to be much greater than unity at the edge of the plasma and greater than unity over a significant portion of the plasma.

The effect of a conducting wall on the stability of m = 1 modes according to our calculations follows the predictions of Shafranov, /7/, as long as the plasma is restricted to N being close to unity. For the higher values of N, however, due to the localization of the eigenfunctions in the Suydam unstable region the effect of the wall on m = 1 modes will be negligible. This concerns, of course, the current density profiles of types III and IV. This behaviour is

consistent with that which has been observed for high-β screw pinch plasmas /4/. As mentioned earlier, the picture is considerably different for the $m \geq 2$ modes with respect to the effect of the conducting wall. The conducting wall has a noticeable, but small, effect on $m = 2$, smaller for $m = 3$ and so forth for $m \geq 4$ for profiles of type I and II. The effect is much smaller than that predicted by Shafranov and is due to the more localized behaviour of the eigenfunctions which we have calculated in comparison with those of /7/. We can qualitatively explain this behaviour in the following manner. The modes which we are examining are primarily current driven modes and should be localized where the driving forces are localized. The localization of the $m \geq 2$ modes follow this simple picture and it is clear that this is true from the eigenfunctions shown for $m = 2$ and 3 for profile IV in figure 13. Recently, experiments with the T-6 Tokomak at Kurchatov Institute, /27/, have been performed with various positions of the perfectly conducting wall with respect to the radius of the plasma. It was noticed that the tendency towards stability occured as the wall was brought closer to the plasma but only up to a certain point due possibly to spurious plasma-wall interaction. The effect was not as great as that predicted by Shafranov, /7/. It was inferred that the current density profiles were not of the peaked type. Further experimentation is necessary to fully determine whether or not the conducting wall plays an important role for $m \geq 2$. The present indications are that, if there is an effect, it will not be a large one.

A further calculation of Shafranov's,/7/, shows that it is possible to find a current density profile, peaked on the axis, which will stabilize $m \geq 2$ modes. This is possibly an effect due to the assumption of $k^2 r^2 \ll m^2$ and indicates that the $m \geq 2$ unstable mode spectrum is being shoved outside the domain of validity of the theoretical analysis. Since we consider all k's, we never lose the unstable $m \geq 2$ modes. This is very important for, even though the $m \geq 2$ modes in our model are found for the larger values

of $\tilde{k}$ or N the more peaked the current distribution, there is a simple physical mechanism which shifts the spectrum back down to lower $\tilde{k}$'s or N's. The explanation of this mechanism now follows.

First we mention that all experimental observations of $m > 2$ perturbations in Tokomak plasmas were accompanied by the additional observation that the perturbations were rotating in the poloidal direction, /14, 22/. Furthermore it was determined that the $m \geq 2$ modes all rotated at the same frequency f/m, where f was the observed signal frequency and m the mode number. This indicates that there is superimposed on the equilibrium a background rotation of the plasma column in the poloidal direction. Rotation gives rise to centrifugal forces which can be destabilizing. We have included the effect of a rigid rotation on the plasma equilibrium for our model plasma and the new governing equations are given in the appendix. We have not solved the new set of equations including rotation, however, we indicate by comparison with another similar problem what the expected effect of rotation should be. Freidberg and Wesson, /28/, have considered the stability of a rotating infinitely long cylindrical theta pinch which, in the absence of rotation, is absolutely stable to $m \geq 1$ modes for all wavenumbers. Inclusion of rotation triggers the $m = 1$ mode leaving $m = 1$, $k = 0$ marginally stable. Furthermore, $m \geq 2$ modes become unstable and the envelopes of growth rate versus k are nested and localized about $k = 0$. That is, for a given value of k a finite number of m modes are simultaneously unstable. Although we cannot at this point say how this will appear in the present problem we make the plausible argument that, due to rotation, the $m \geq 2$ mode spectrum for our Tokomak model plasma will be shifted toward lower N values. Depending on how this occurs, it is then plausible that mode mixing at low values of N may occur. In any case it seems plausible that with rotation $m \geq 2$ modes should be observable at small N; indeed $N = 1$ is observed in the experiments, /14, 22/.

VI. Conclusions and recommendations

We have shown that the consideration of realistic current density profiles and a more exact treatment of MHD stability leads to results which can be considerable different from those previously obtained. By numerically integrating the linearized ideal MHD equations of motion more detailed and informative results can be obtained than by using the energy integral together with restrictive expansions and arbitrary test functions. We find for a cylindrical Tokomak-like plasma with a peaked on axis current distribution that $q = 1$ at the limiter is not the stability condition but that q must be much greater than unity for stability to $m = 1$ perturbations. Further it is shown that a conducting shell has a negligible effect on $m \geq 2$ modes for an on-axis peaked current distribution.

It was shown by calculation and by comparison with similar problems that higher m mode mixing is possible.

Further studies should be concerned with the following points:

1) For given experimental parameters, i.e. those of ST, T-6, ORMAK, etc., the MHD stability analysis should be carried out for the various m modes including effects of rotation.

2) An attempt should be made to simulate the toroidal effect of suppressing certain localized modes, possibly by suppressing the pressure driven terms in the governing equations.

VII. Acknowledgements

The authors would like to thank Dr.GlennBateman for useful discussions and his constant reminder that we read the literature. One of us (s.o.) would like to thank Professors E.Fünfer and H.Zwicker for their kind hospitality while he was a guest at the Max-Planck-Institute.

Appendix A

In this section we give the correction to the governing set of equations which are necessary to include the effect of a rotation of the equilibrium plasma column. Instead of a static equilibrium we now describe the unperturbed plasma state by the following:

$$B_o = (0, B_{\theta_o}, B_{z_o}), \qquad A - 1$$

$$V_o = (0, V_{\theta_o}, 0), \qquad A - 2$$

$$P_o = P_o(r) \qquad A - 3$$

$$\rho_o = \rho_o(r) \qquad A - 4$$

where V_o represents the equilibrium velocity. We allow only a velocity in the θ-direction and for simplicity here choose the special case of rigid plasma rotation, $V_{\theta_o} = r\Omega$ where Ω is a constant rotational frequency. Proceeding as before, we linearize the ideal MHD incompressible equations of motion and assume here that all perturbation quantities have the form:

$$\phi \sim \phi(r) \exp\left[i\,(\omega t + \underline{k} \cdot \underline{r})\right], \qquad A - 5$$

where ϕ represents any perturbation quantity. In exactly the same manner as before we solve for the radial velocity perturbation eigenfunction U_r in terms of a second order differential equation which is given as:

$$\left[\frac{\tilde{A}\, r}{m^2 + k^2 r^2}\left(r\, U_r\right)'\right]' + \left[-\frac{\tilde{A}}{r} - \Omega^2 \rho_o' + \right.$$

$$\left. \frac{4\,\rho_o^2\,\Omega^2\,\sigma^2\,k^2\,r}{\tilde{A}\,(m^2 + k^2 r^2)} + \frac{4\,F^2 B_{\theta_o}\,k^2}{\mu_o\, r\,\tilde{A}(m^2+k^2r^2)} + \frac{2\,B_{\theta_o}}{\mu_o\, r}\left(\frac{B_{\theta_o}}{r}\right)'\right.$$

$$+ \frac{8\,\rho_o\,\Omega\,\sigma\,F\,B_{\theta_o}\,k^2}{\mu_o\,\tilde{A}\,(m^2+k^2r^2)} - 2\sigma\,m\,\Omega\left(\frac{\rho_o}{m^2+k^2r^2}\right)' - \frac{2\,m}{\mu_o}\left(\frac{F\,B_{\theta_o}}{r\,(m^2+k^2r^2)}\right)'\Big]\,(r\,U_r) = 0. \qquad A - 6$$

Identically the same boundary conditions as on ξ_r apply to U_r. In A - 6 the following definitions apply:

$$\tilde{A} = -\rho_o\,\sigma^2 + \frac{F^2}{\mu_o}, \qquad A - 7$$

$$\sigma = \omega - m\,\Omega\,. \qquad A - 8$$

The growth rate γ is defined as $-i\omega$ and can be shown to be complex. Setting B_{θ_o} equal to zero in A - 6 results in the equation valid for a pure linear θ-pinch and is the equation studied by Freidberg and Wesson /28/.

References

/1/ Green,J.M., J.L.Johnson, Phys.Fluids 5, 510 (1962)

/2/ Robinson,D.C., Plasma Phys. 13, 439 (1971)

/3/ Robinson,D.C., IPP-Report* 1/127 (1972), paper C 1

/4/ Grossmann,W., Proc.of the 4th Europ.Conf.on Contr. Fusion and Plasma Physics, p. 48, Rome (1970).

/5/ Freidberg,J., B.M.Marder, Phys.Fluids 1, 174 (1971)

/6/ Dimock,D.L., et.al., Princeton Plasma Physics Laboratory report MATT-906, July 1972.

/7/ Shafranov,V.D., Soviet Phys-Tech.Phys., Vol.15,No.2, 175,(1970)

/8/ Kruskal,M.D., M.Schwarzschild, Proc.Roy.Soc.(London) A 223, 348 (1954)

/9/ Shafranov,V.D., J.Nuclear Energy (pt.C) 10, 86 (1957)

/10/ Weitzner,H., Phys.Fluids 3, 658 (1971)

/11/ Freidberg,J.P., Phys.Fluids 14, 2454 (1971)

/12/ Bateman,R.G., Physics Fluids 14, 1506 (1971)

/13/ Freidberg,J.P., Phys.Fluids 15, 1102 (1972)

/14/ Mirnov,S.V., I.B.Semenov, Sov.Phys.JETP, Vol.33,1134 (1971)

/15/ Tataronis,J.A., W.Grossmann, Bull.APS, Series II, Vol.16, No.11, page 1293 (1971)

/16/ Goedbloed,J.P., H.J.L.Hagebeuk, Phys.Fluids 15, 1090 (1972)

/17/ Freidberg,J.P., Phys.Fluids 13, 1812 (1970)

/18/ Tayler,R.J., Proc.Phys.Soc. (London) B 70, 1049 (1957)

/19/ Crow,J.E., D.C.Robinson, IPP-Report* 1/127 (1972) paper C 1

/20/ Grossmann,W., Univ.Padua, report uPee -72/07 (1972)

/21/ Ortolani,S., W.Grossmann, 3rd Int.Toroidal Plasma Confinement Conf., Garching, March 26-3o, 1973 paper F 8.

/22/ Hosea,J.C., C.Bobeldijk, D.J.Grove, Princeton Univ., MATT-855 (1971)

/23/ Rutherford,P.H., Proc. of the 3rd Intern. Symposium on Toroidal Plasma Confinement, Garching, March 26-3o, 1973 paper B 2

/24/ Rosenbluth,M.N., R.Dagazian, P.H.Rutherford, ibid, paper B 3.

/25/ Furth,H.P., ibid, paper B 9

/26/ Jobes, F.C., J.C.Hosea, ibid, paper B 14

/27/ Vlasenkov, V.S., et al., ibid, paper B 2

/28/ Freidberg,J.P., J.A.Wesson, Phys.Fluids 13, 1117 (1970)

---

* proceedings of 2nd Topical Conference on Pulsed High-Beta Plasmas, Garching, July 6-9, 1972.

Figure Captions

1) The normalized current density profiles.

2) The function $f_2(\tilde{r})$ as a function of $\tilde{r}$ for the different current density profiles.

3) The variation of q over radius for the different current density profiles.

4) The radial variation of position of singular surfaces as a function of wavenumber: superposition of regions where the Suydam criterion is violated.

5) The ν versus k spectrum for constant pitch, incompressible m = 1 modes.

6) The γ versus k spectrum for m = 1 for profiles I,II,III and IV. The curves are computed for both fixed boundary (dashed curve joining the right hand portion) and free boundary (full curves) cases.

7) Variation of growth rate as a function of the external density ratio.

8) m = 1 radial eigenfunction for profile IV; free and fixed boundary cases.

9) Typical m = 1 eigenfunctions for the profiles I - IV, fixed boundary case.

10) The spectrum of unstable m = 1,2 modes for profile II, μ = 0.2.

11) The radial eigenfunction for the m = 2 mode for profile II, μ = 0.2.

12) The spectrum of unstable modes for profile IV for m = 1,2 and 3 modes" μ = 0.2.

13) The radial eigenfunctions for m = 2 and 3 for profile IV, μ = 0.2.

14) The m = 1 growth rate $\tilde{\gamma}$ as a function of $\tilde{k}$ for the fixed boundary profile IV case.

15) The m = 1 eigenfunctions as a function of μ for profile IV.

16) The m = 1 growth rate γ as a function of k for the fixed boundary profile IV case.

17) Maximum growth rate for m = 1, profile IV, as a function of μ.

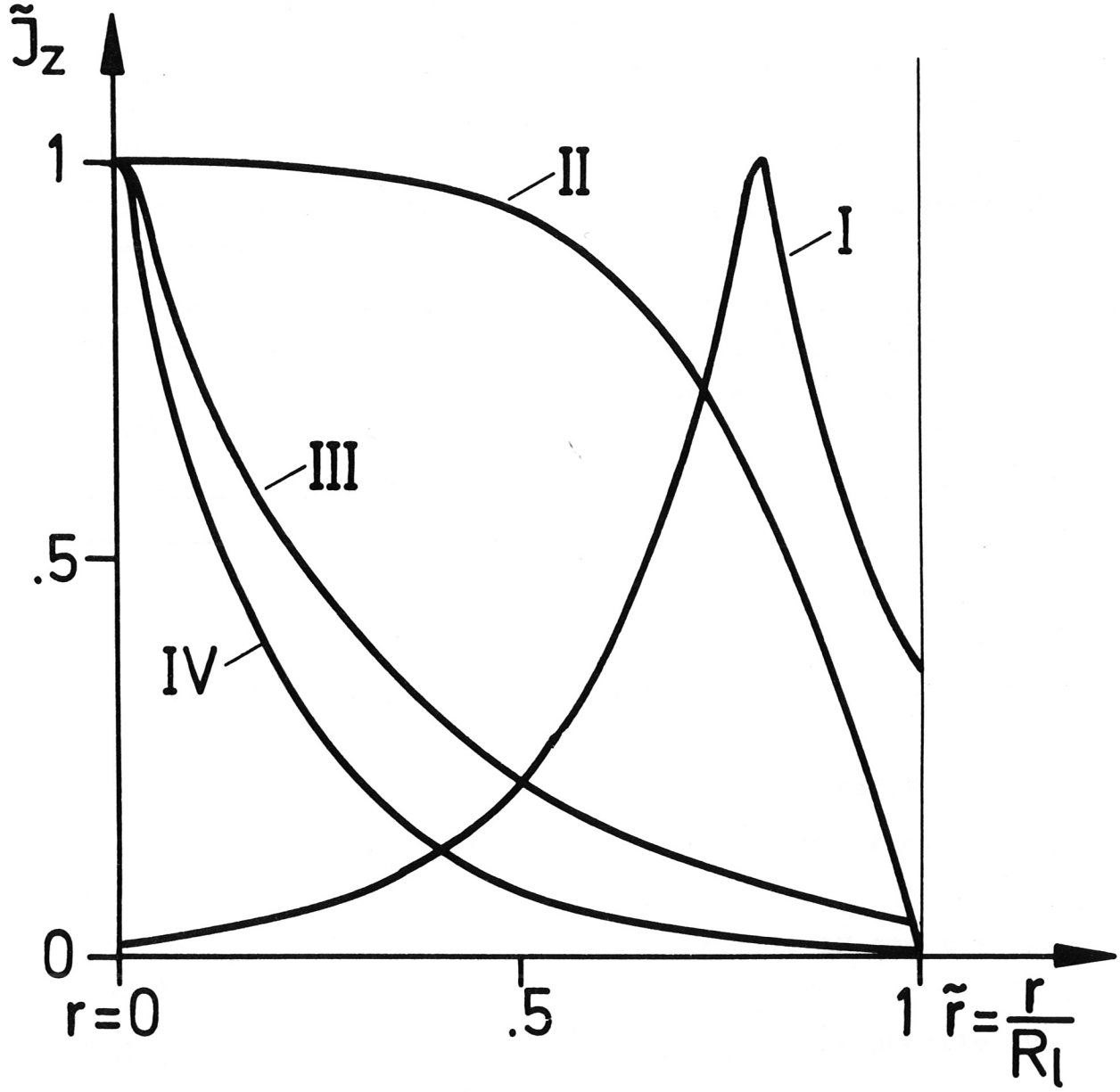

Fig. 1

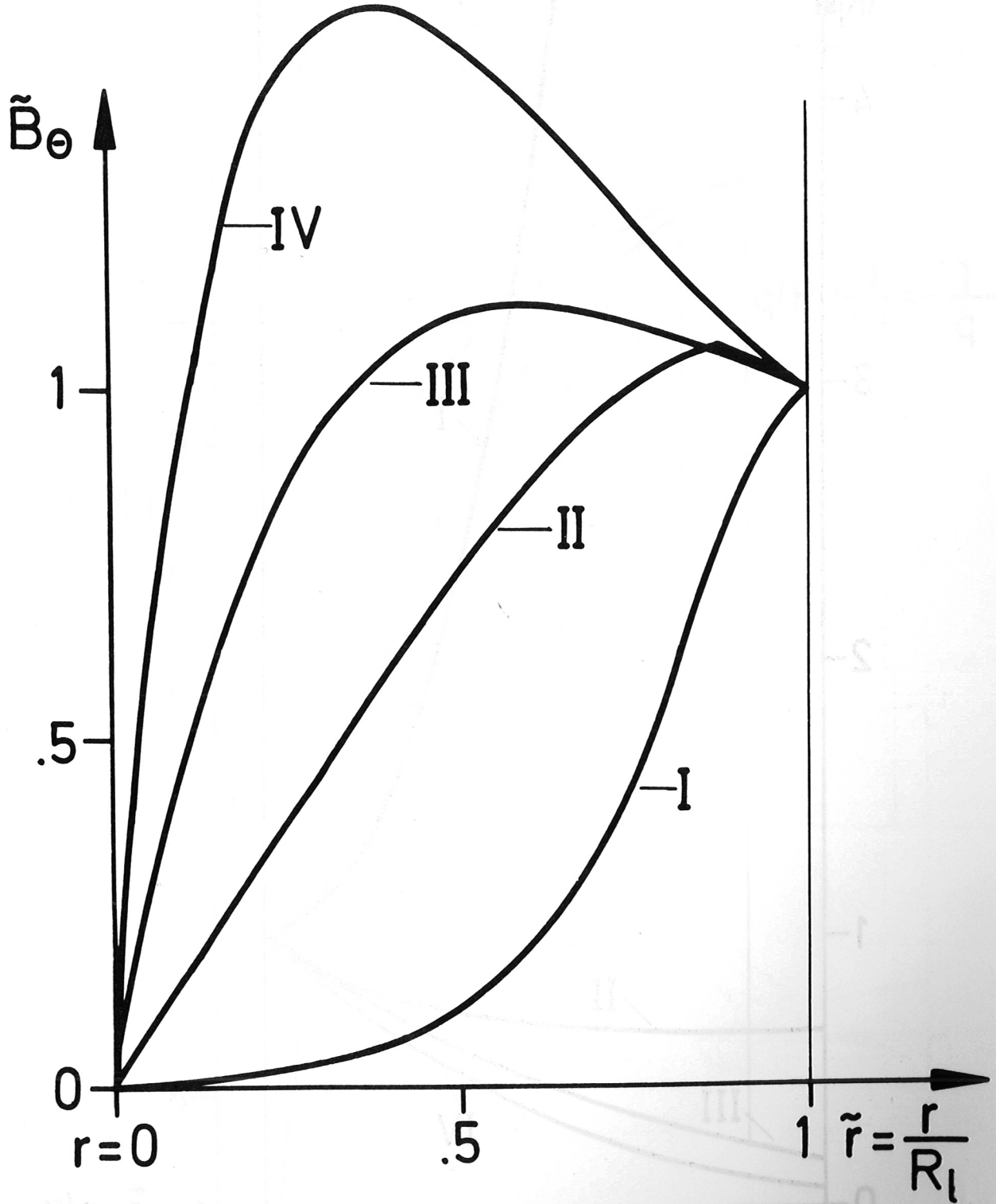

Fig. 2

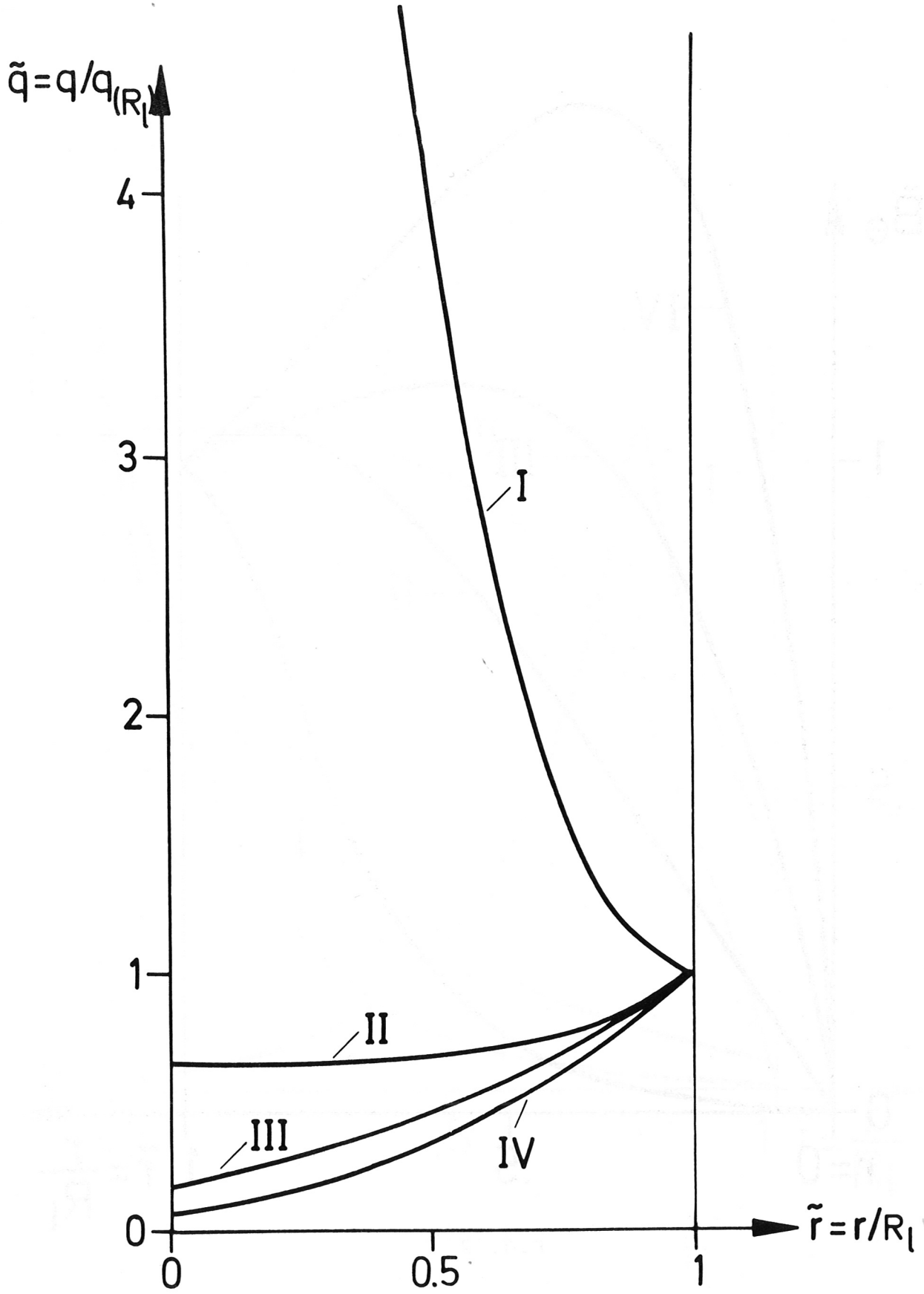

Fig. 3

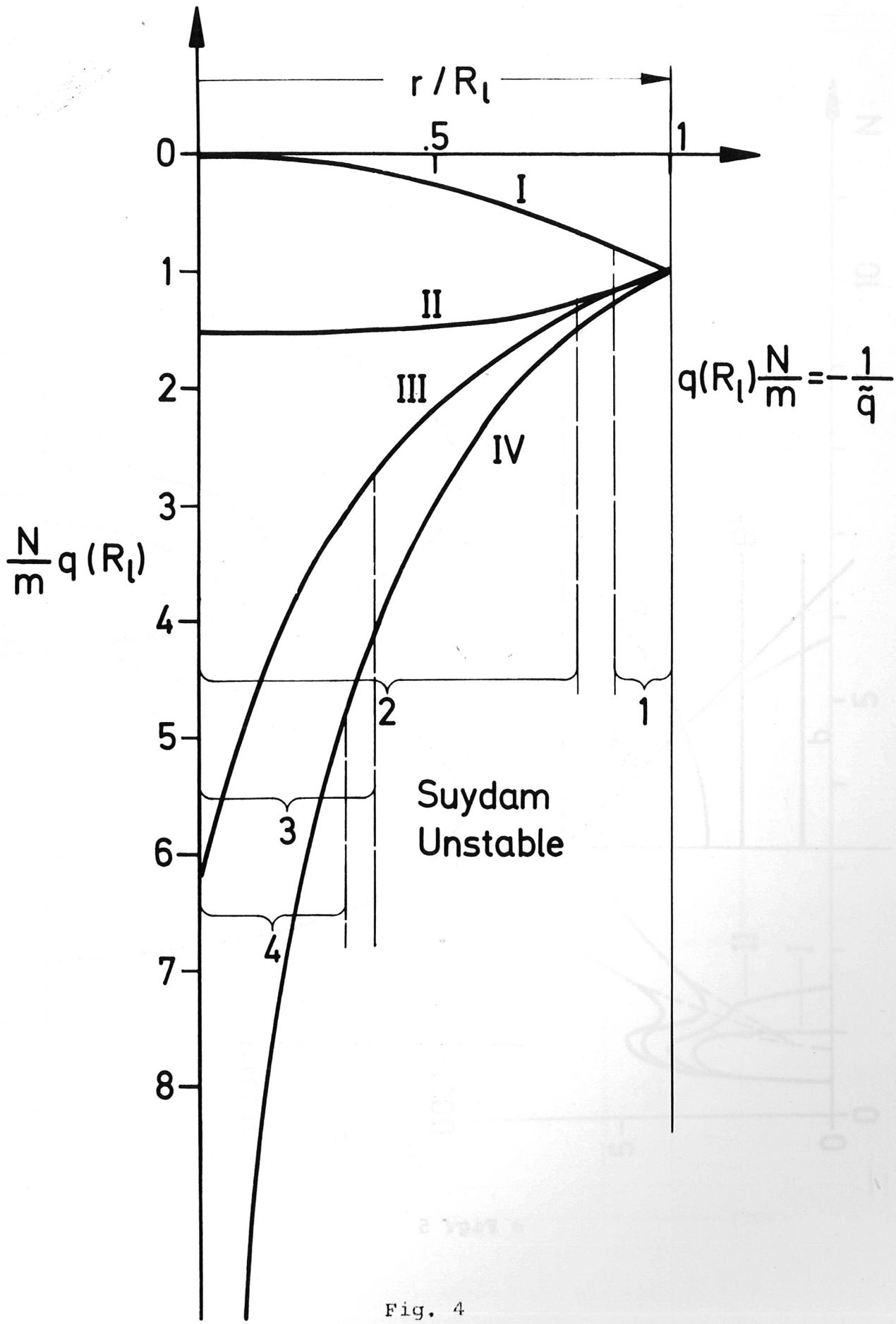
r / R_l
.5
1
0
I
1
II
2
III
IV
3
N/m q(R_l)
4
5
6
7
8
q(R_l) N/m = -1/q̃
2
1
3
4
Suydam
Unstable

Fig. 4

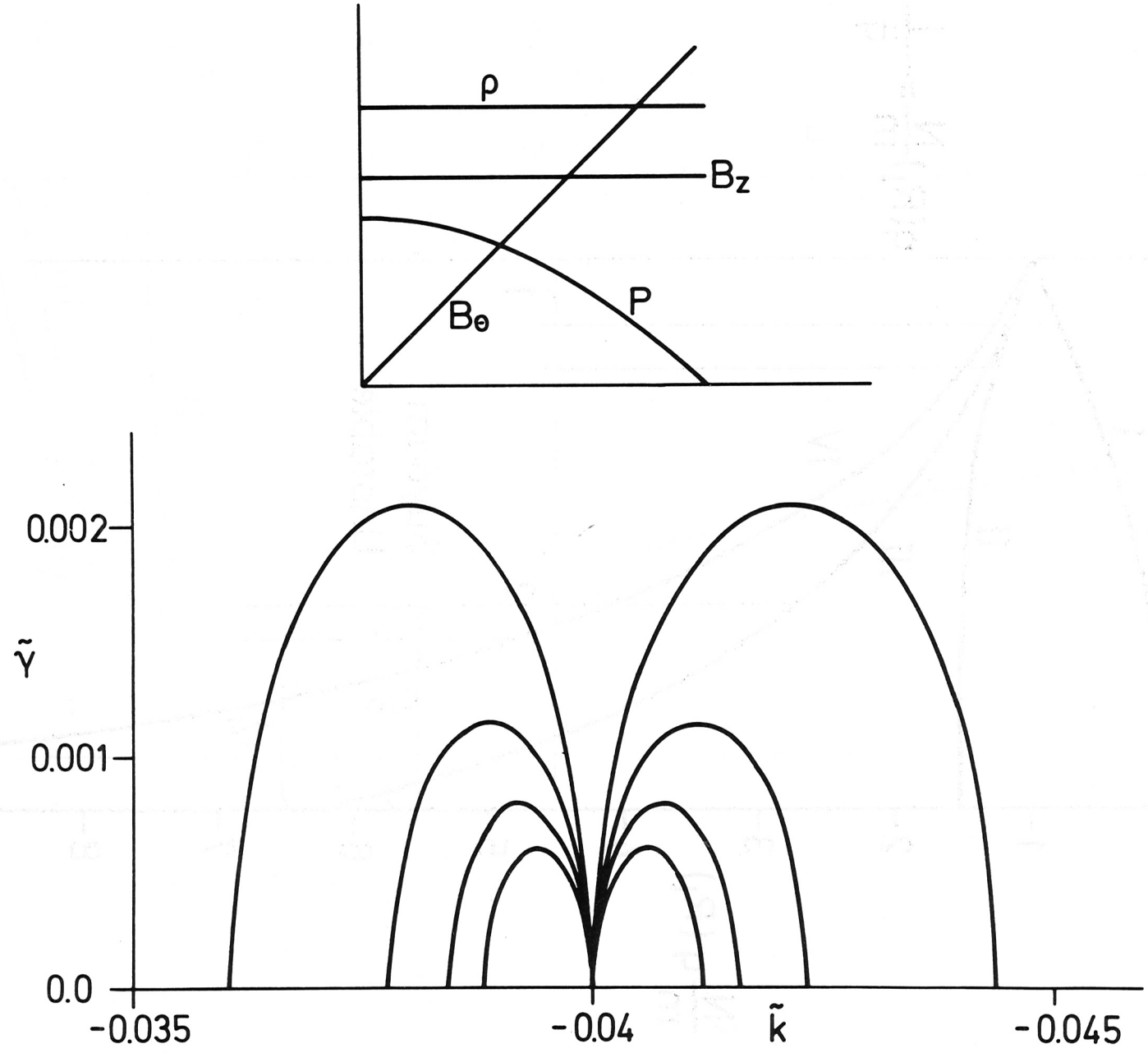

Fig. 5

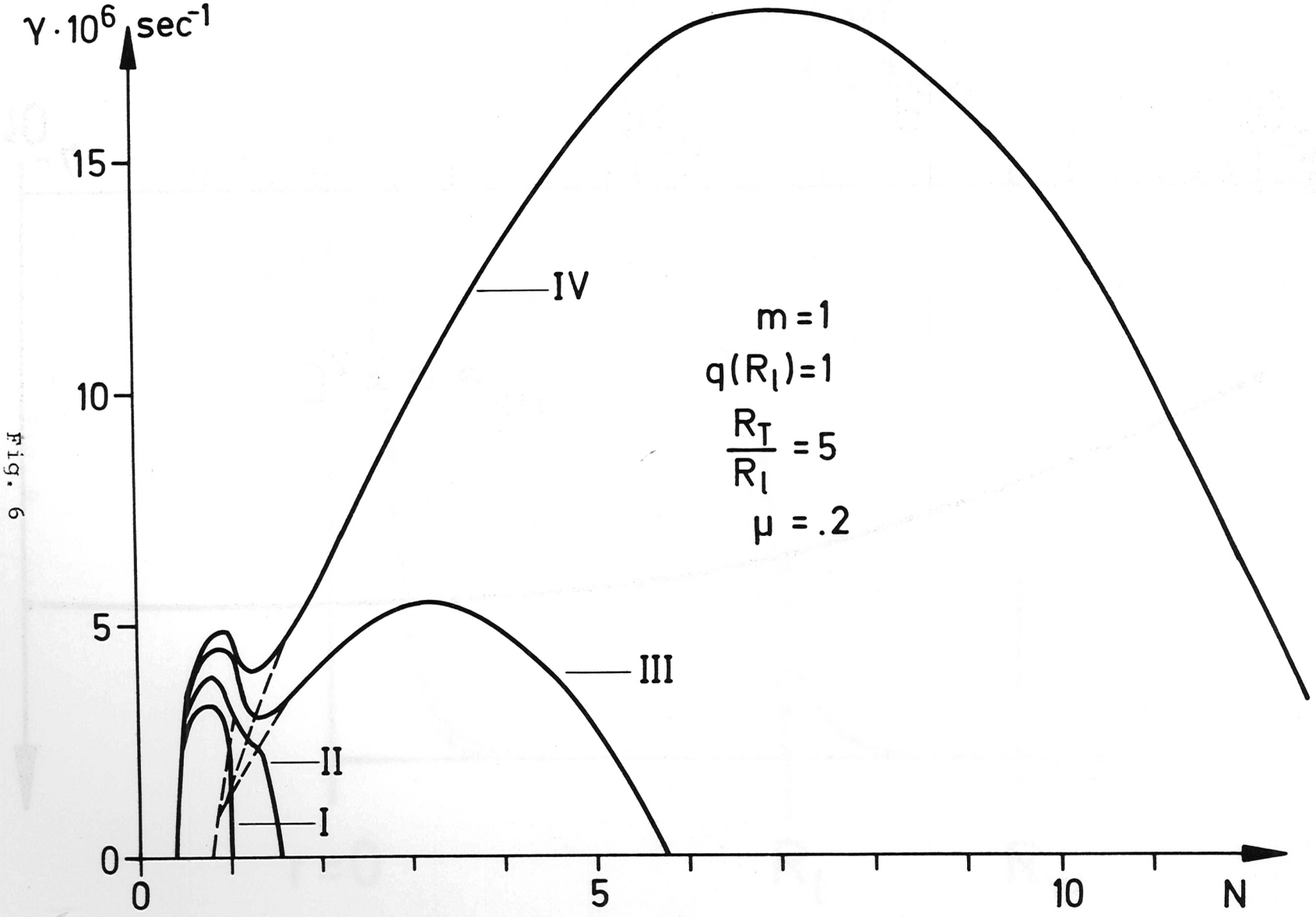

Fig. 6

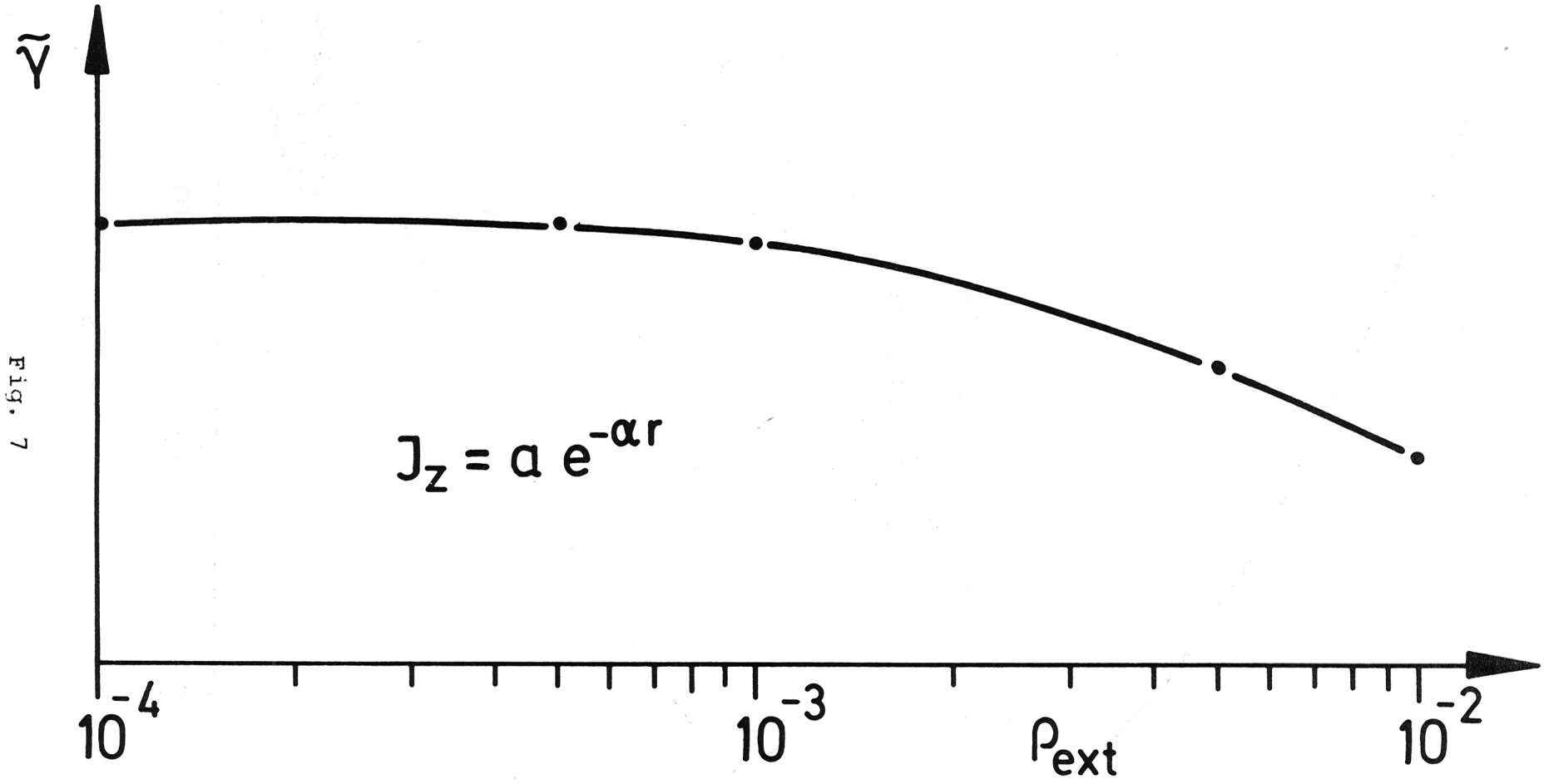

Fig. 7

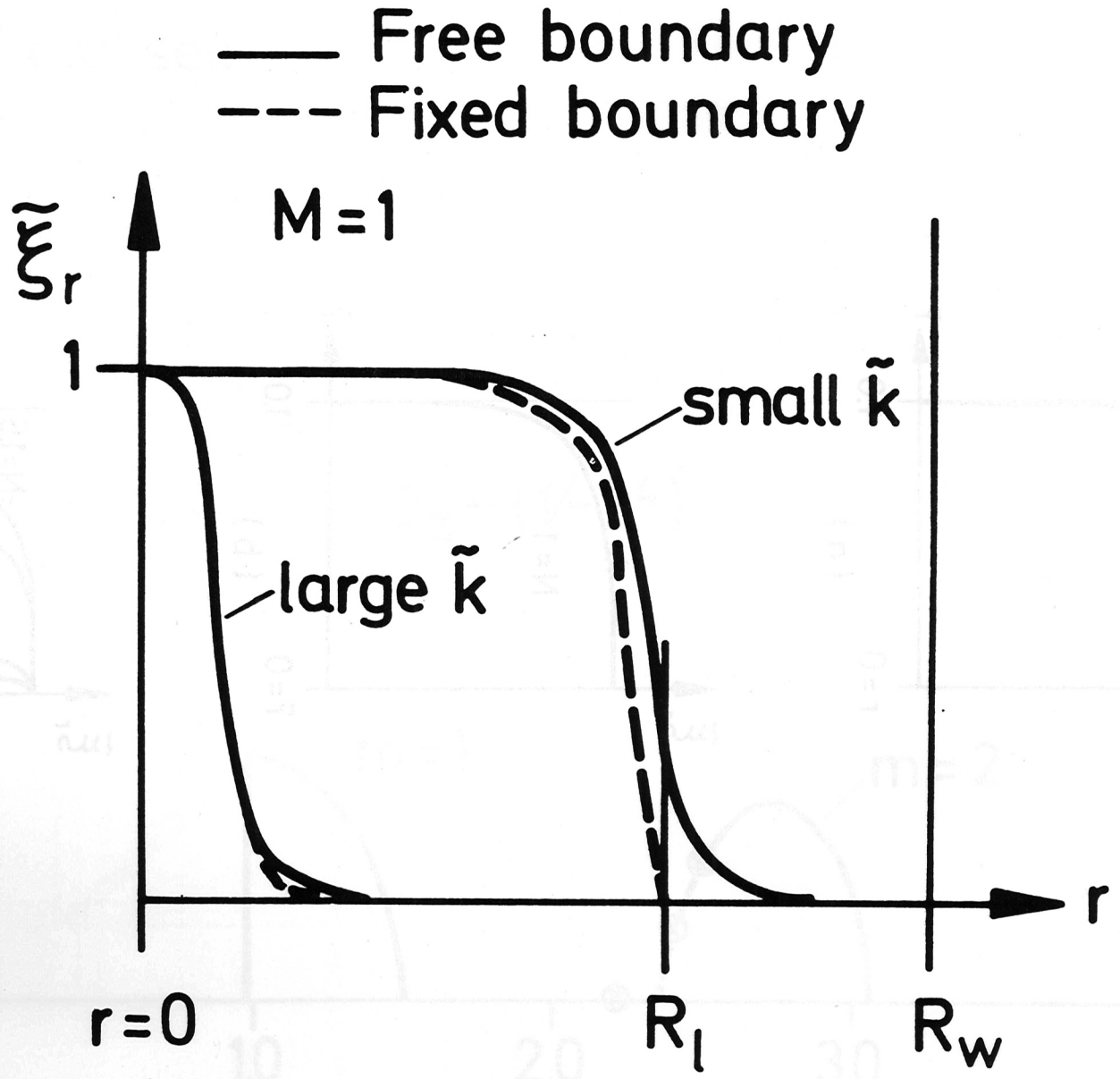
Free boundary
Fixed boundary
M=1
$\tilde{\xi}_r$
1
small $\tilde{k}$
large $\tilde{k}$
r
r=0
R_l
R_w

Fig. 8

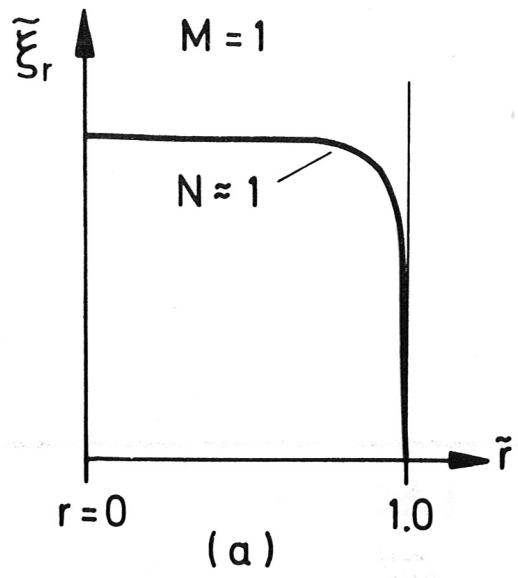
$\tilde{\xi}_r$
M = 1
N ≈ 1
$\tilde{r}$
r = 0
1.0
(a)

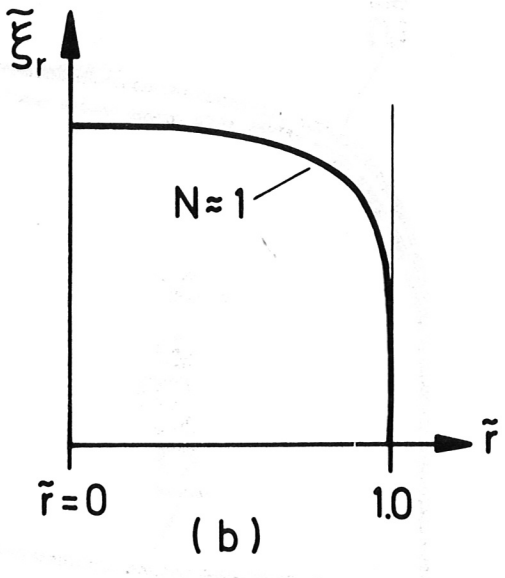
$\tilde{\xi}_r$
N ≈ 1
$\tilde{r}$
$\tilde{r}$ = 0
1.0
(b)

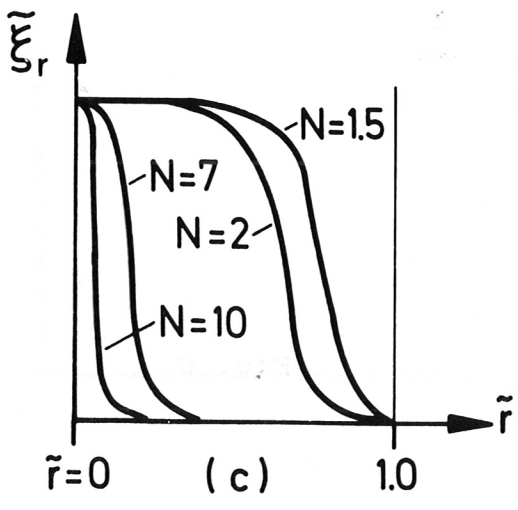
$\tilde{\xi}_r$
N=1.5
N=7
N=2
N=10
$\tilde{r}$
$\tilde{r}$=0
(c)
1.0

Fig. 9

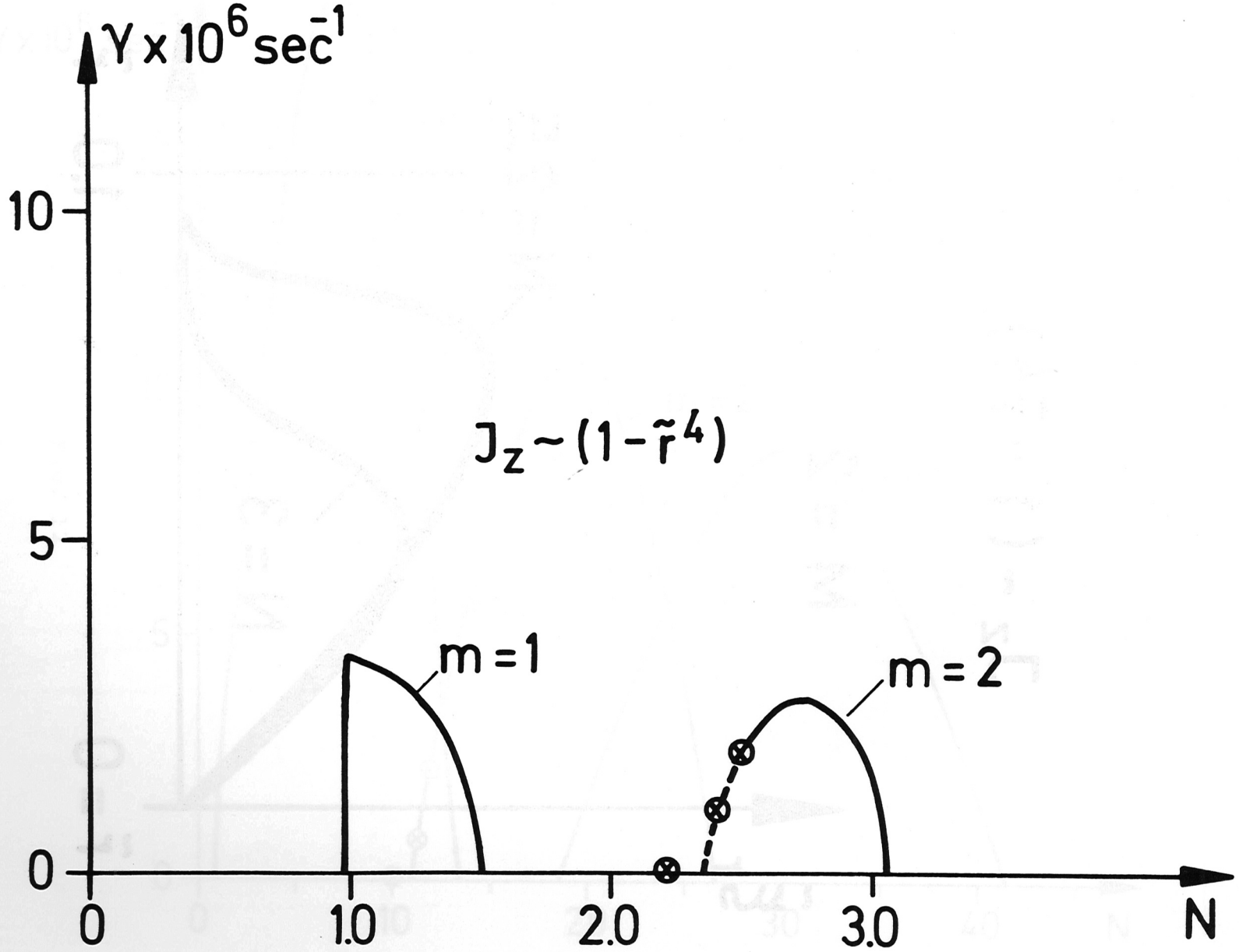

Fig. 10

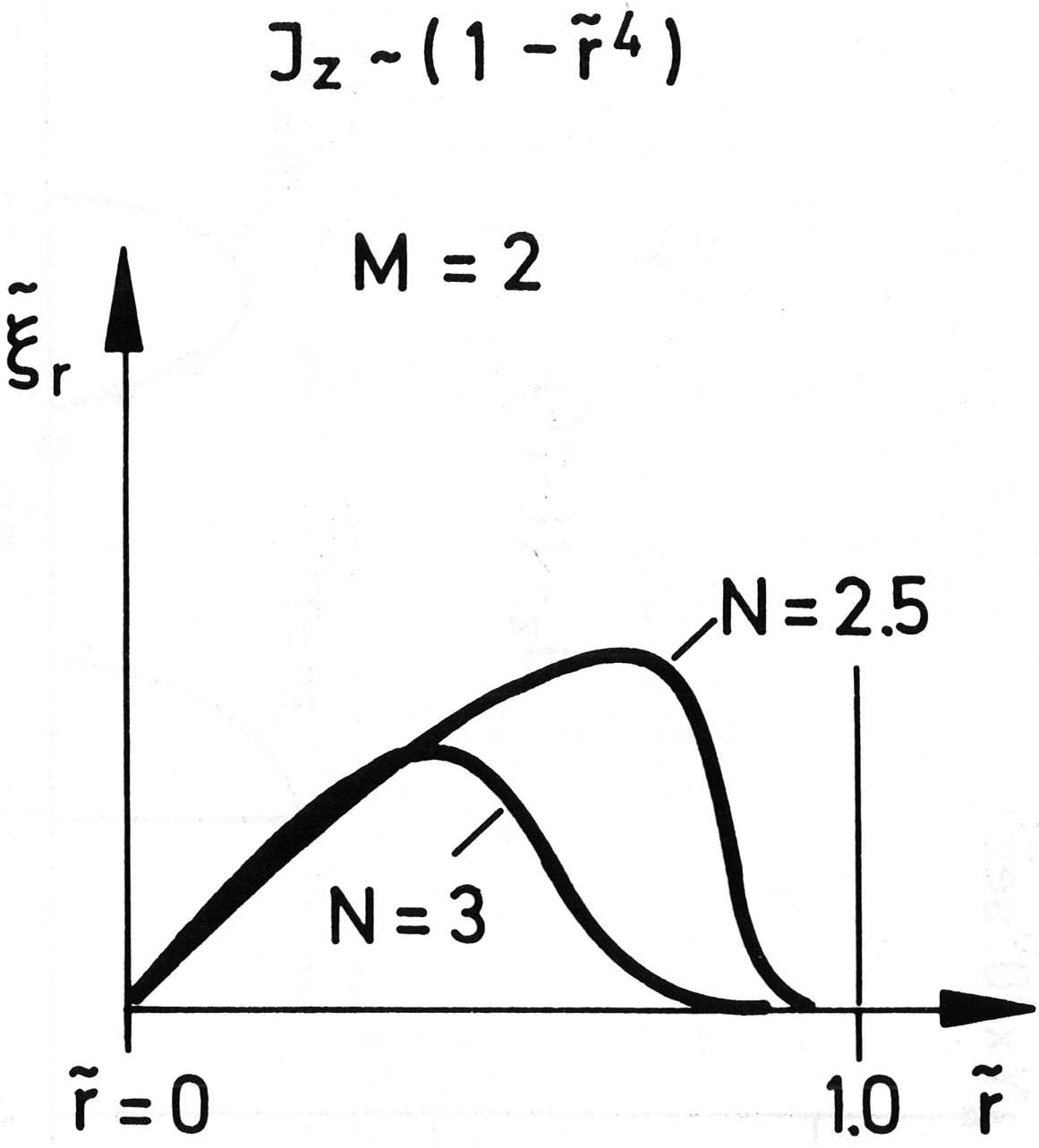

Fig. 11

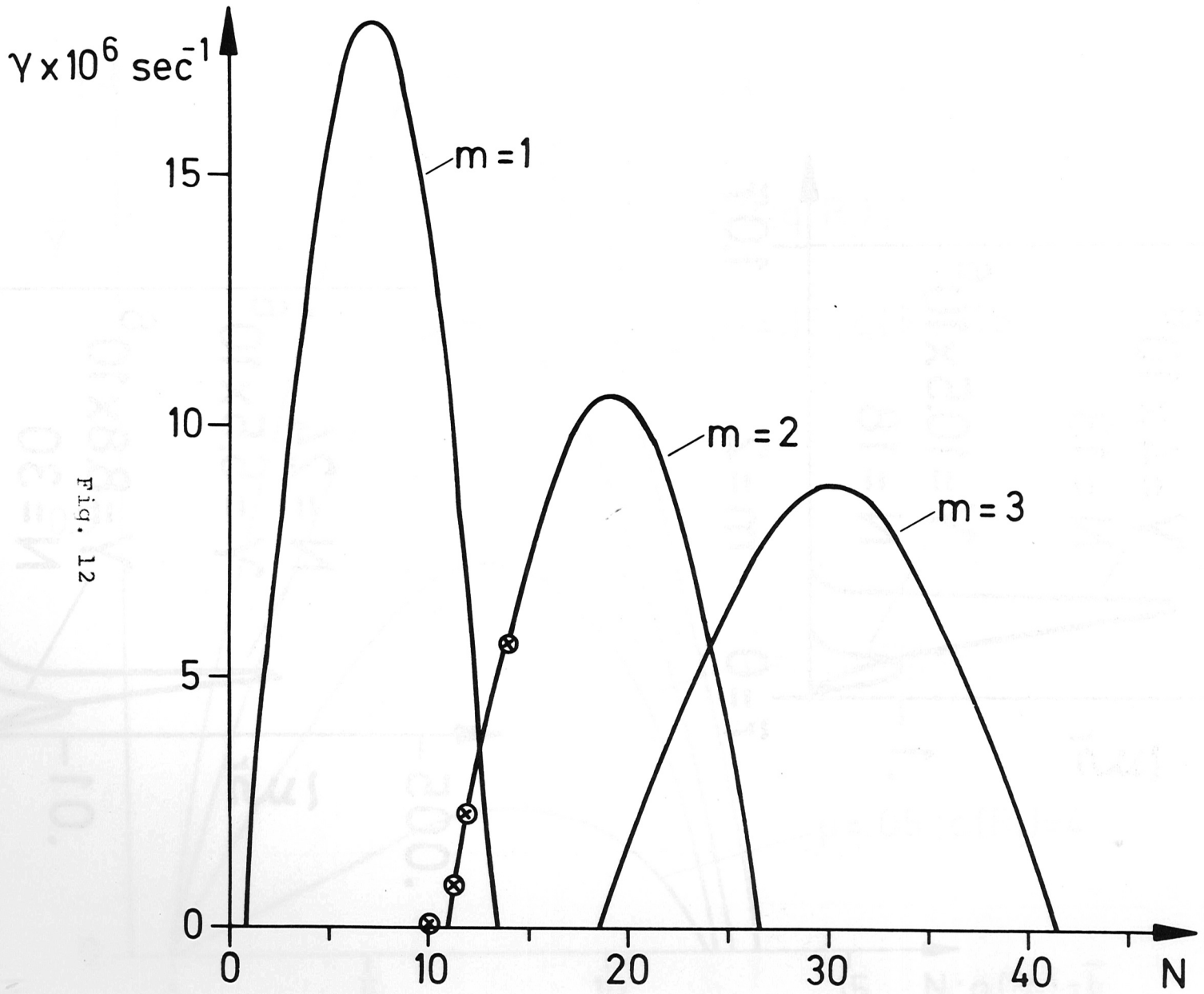

Fig. 12

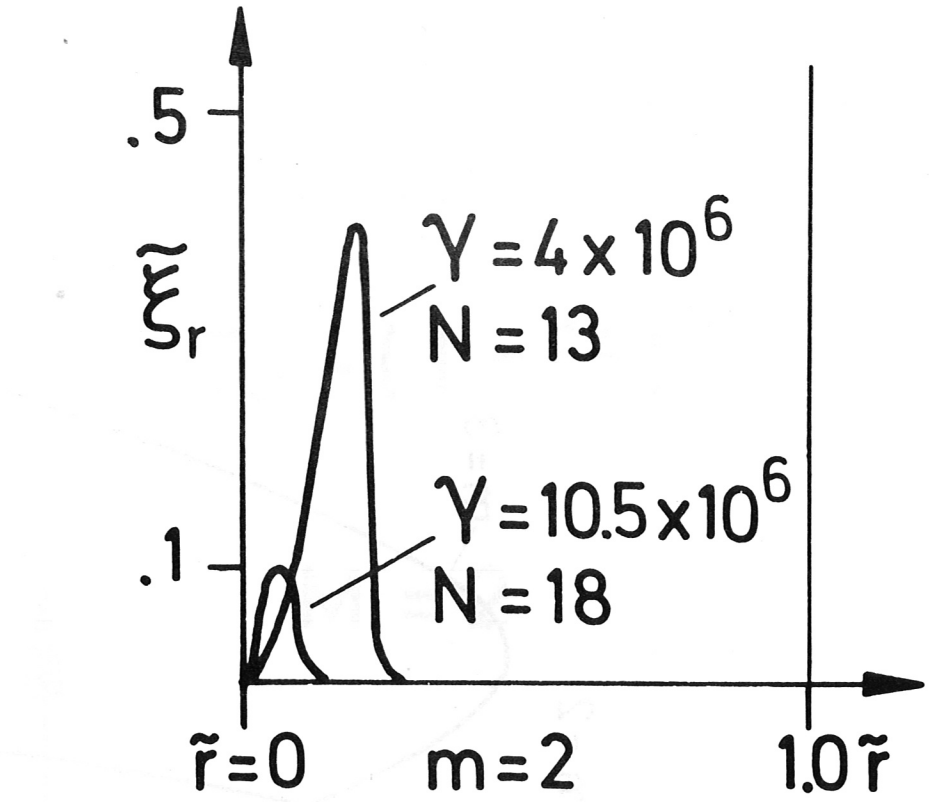
.5
$\tilde{\xi}_r$
.1
$\gamma = 4 \times 10^6$
N = 13
$\gamma = 10.5 \times 10^6$
N = 18
$\tilde{r}=0$
m=2
1.0 $\tilde{r}$

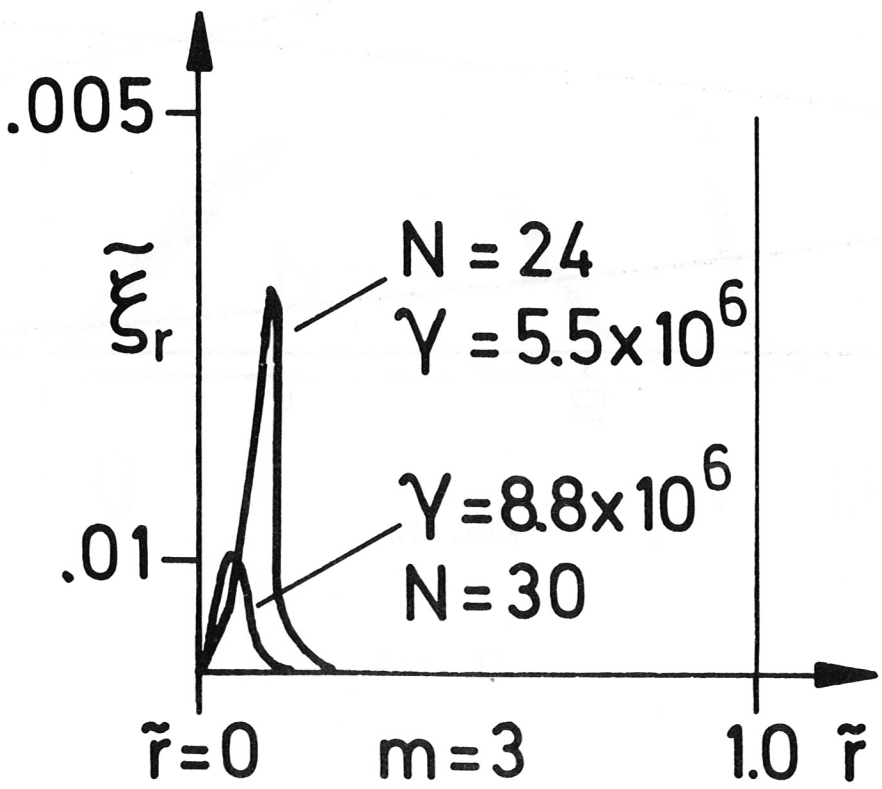
.005
$\tilde{\xi}_r$
.01
N = 24
$\gamma = 5.5 \times 10^6$
$\gamma = 8.8 \times 10^6$
N = 30
$\tilde{r}=0$
m=3
1.0 $\tilde{r}$

Fig. 13

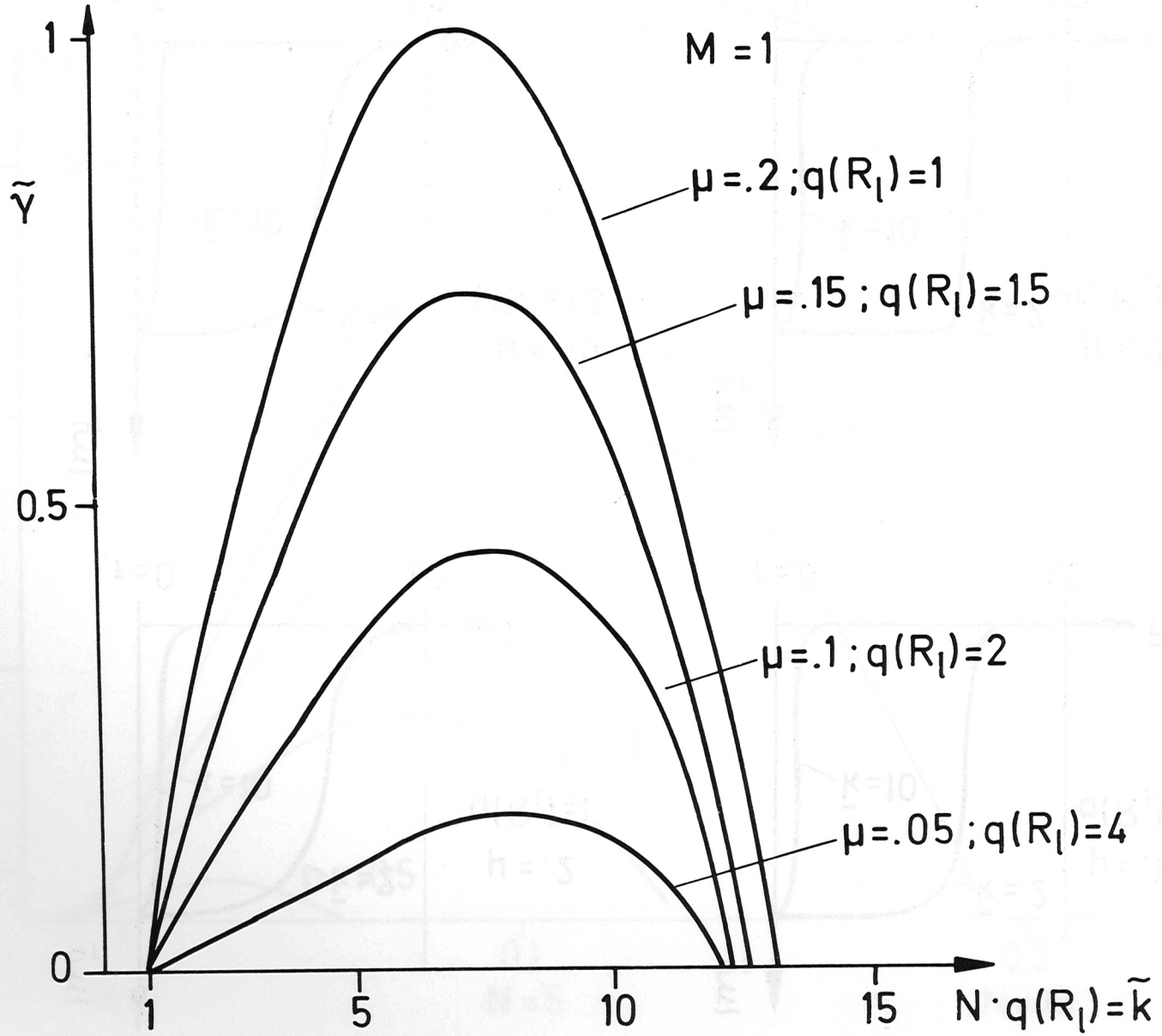

Fig. 14

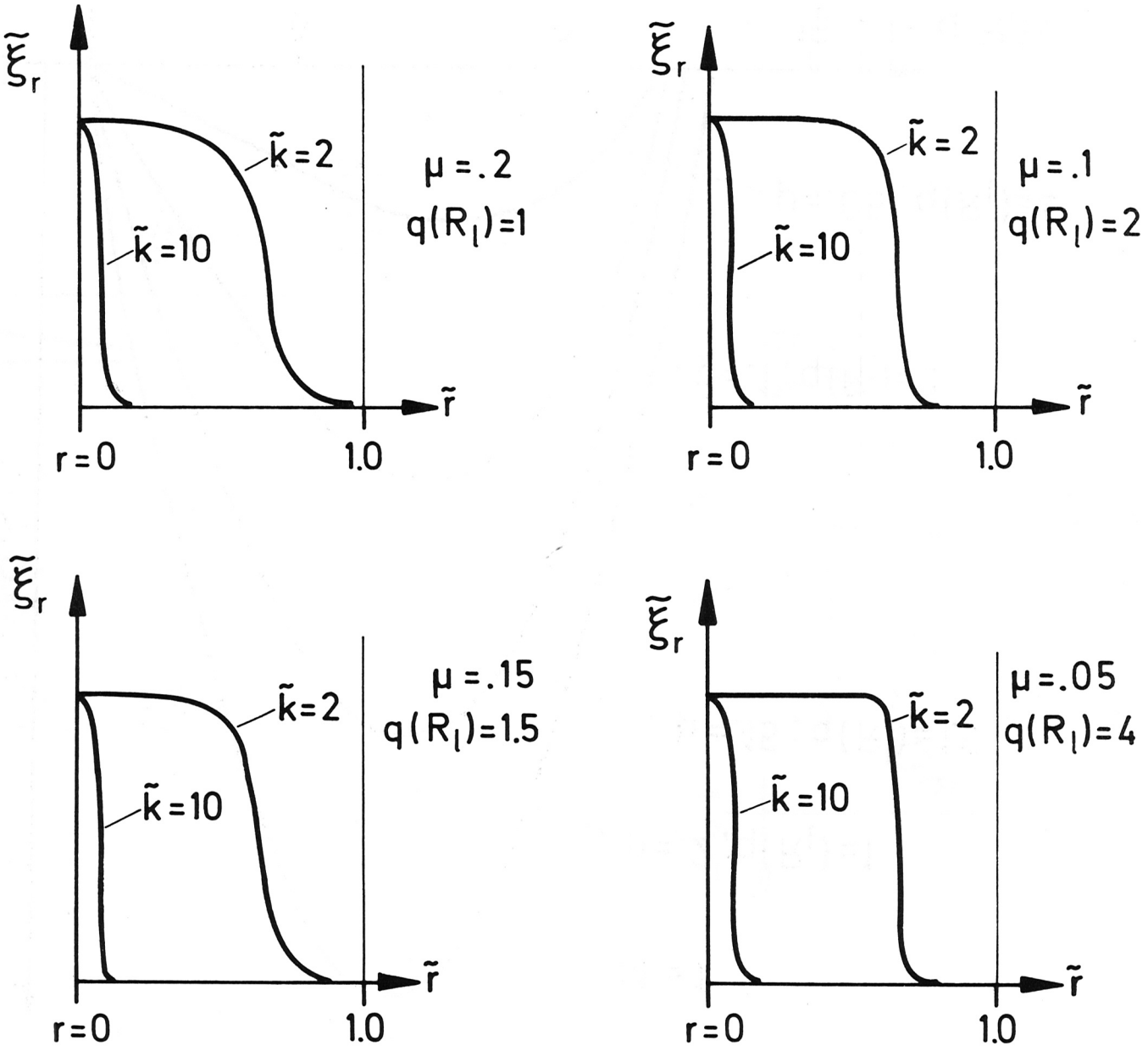
$\tilde{\xi}_r$
$\tilde{k}=2$
$\tilde{k}=10$
$\mu=.2$
$q(R_l)=1$
$\tilde{r}$
r=0
1.0
$\tilde{\xi}_r$
$\tilde{k}=2$
$\tilde{k}=10$
$\mu=.1$
$q(R_l)=2$
$\tilde{r}$
r=0
1.0
$\tilde{\xi}_r$
$\tilde{k}=2$
$\tilde{k}=10$
$\mu=.15$
$q(R_l)=1.5$
$\tilde{r}$
r=0
1.0
$\tilde{\xi}_r$
$\tilde{k}=2$
$\tilde{k}=10$
$\mu=.05$
$q(R_l)=4$
$\tilde{r}$
r=0
1.0

Fig. 15

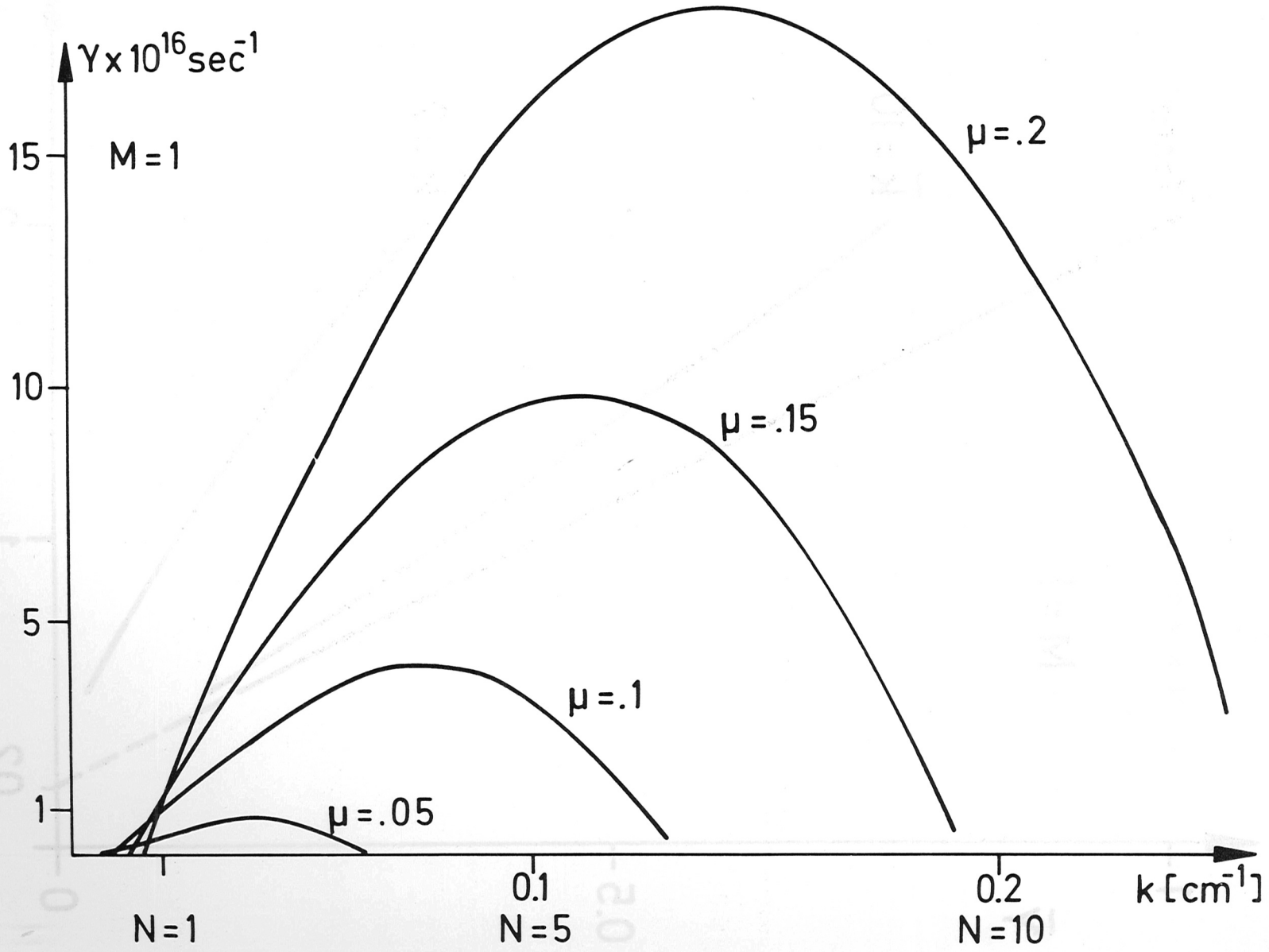

Fig. 16

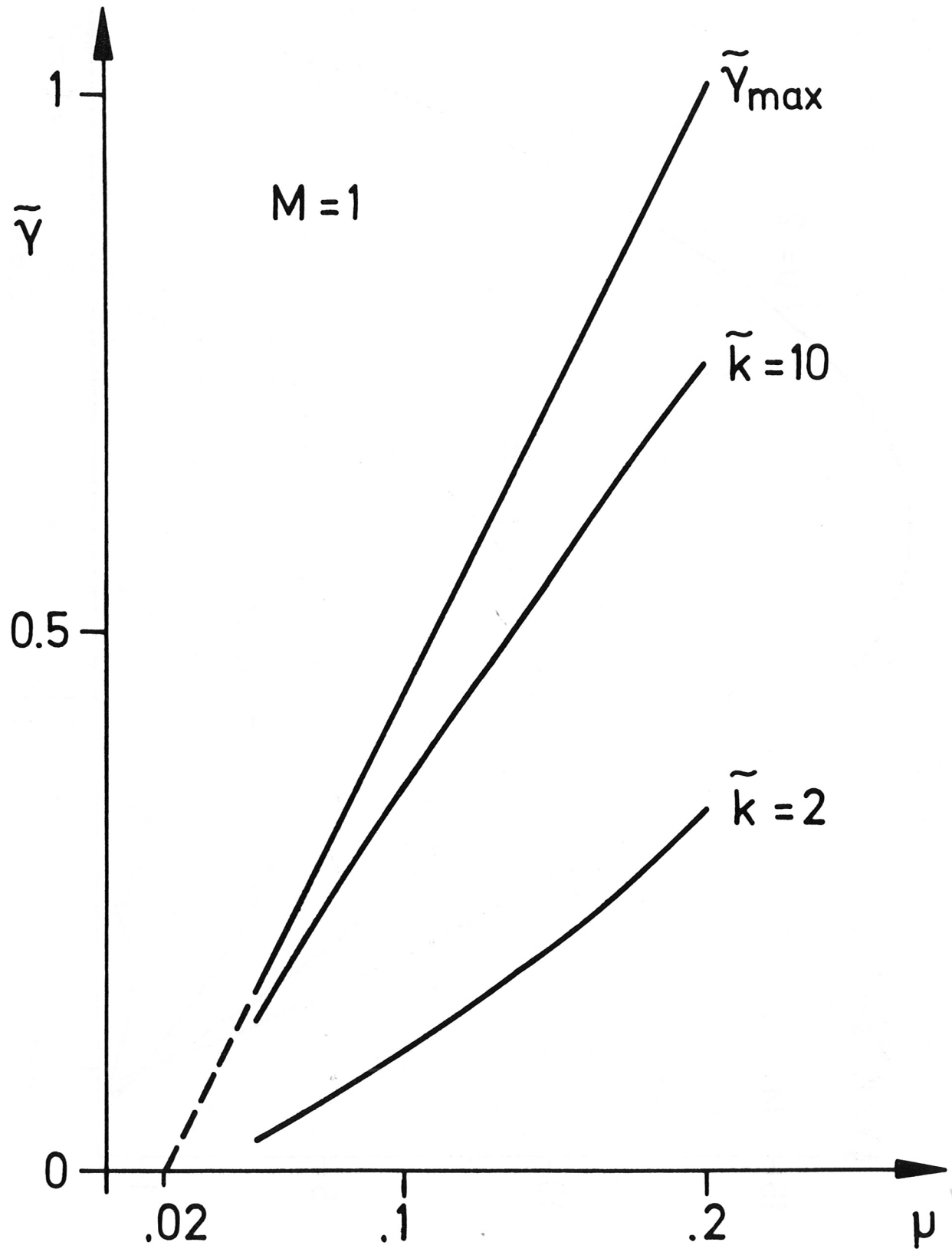

Fig. 17

ERRATA

The vertical scale in figure 16 is $\gamma \times 10^{6}$ sec^{-1}.